# Numerical study of 1+1D drift kinetic models for parallel dynamics in the plasma edge

**M. Barnes[1], F. I. Parra[2], M. R. Hardman[1] and J. Omotani[3]**

[1] Rudolf Peierls Centre for Theoretical Physics, University of Oxford, Clarendon Laboratory, Parks Road, Oxford OX1 3PU, United Kingdom

[2] Princeton Plasma Physics Laboratory, P.O. Box 451, Princeton, New Jersey 08540, United States

[3] Culham Centre for Fusion Energy, Culham Science Centre, Abingdon, Oxon, OX14 3DB, United Kingdom

E-mail: michael.barnes@physics.ox.ac.uk

## 1. Introduction

We expect that two of the biggest challenges in numerically solving drift kinetic equations in the plasma edge are treating the motions of charged particles along the magnetic field line and accounting for the interaction between charged and neutral particles. Both of these physics processes differ considerably depending on whether one is in a region with closed or open field lines: charged-neutral interactions are only likely to be significant in the open field line region nearest the wall, where recycling of particles leads to a relatively large neutral density; and parallel dynamics in the open-field-line region will be strongly modified relative to the core by the fact that electrons stream rapidly along field lines into the walls – thus setting up boundary layers with strong electric fields. Our aim with this report is to: present a set of drift kinetic models as candidate models for describing plasma dynamics parallel to the field in both open-field-line and closed-field-line regions of the edge, in the presence of neutrals; to describe how these models might be implemented numerically; and to test the relative efficacy of these models for numerical simulation.

We start in Section 2 by stating the common assumptions made for all of the models and by presenting the standard drift kinetic model equations for parallel plasma dynamics. We then derive a series of 'moment kinetic' models in Section 3 that utilise modified particle distribution functions and parallel velocity coordinates to separate the evolution of the distribution function from its low-order velocity moments. The boundary conditions imposed on the system are discussed in Section 4 before providing the normalised system of equations for each model in Section 5. The key features of our numerical implementation of the model equations are described in Section 6 before presenting numerical results from our code in Section 7. Finally, we provide our conclusions on the suitability of the models for numerical simulation in Section 8 and discuss future directions for the research.

## 2. Drift kinetics for parallel dynamics

A detailed derivation of the drift kinetic model we consider is provided in a previous report [5]. Here we provide a brief overview of the model for the Reader's convenience. The system we consider consists of a single ion species of charge $e$ and mass $m_i$, a single neutral species of mass $m_n = m_i$, and an electron species modelled as having a Boltzmann response, all immersed in a straight, uniform magnetic field in the $z$ direction. We allow for charge exchange collisions between ions and neutrals and ionisation collisions involving ions, electrons and neutrals, but do not account for intra-species collisions. Finally, we assume that the plasma is homogeneous in the plane perpendicular to the magnetic field.

With these assumptions, our model system of equations describing drift kinetics is one dimensional in both configuration and velocity space:

$$\frac{\partial f_i}{\partial t} + v_\parallel \frac{\partial f_i}{\partial z} - \frac{e}{m_i}\frac{\partial \phi}{\partial z}\frac{\partial f_i}{\partial v_\parallel} = -R_{\text{in}}\left(n_n f_i - n_i f_n\right) + R_{\text{ion}} n_e f_n, \tag{1}$$

$$\frac{\partial f_n}{\partial t} + v_\parallel \frac{\partial f_n}{\partial z} = -R_{\text{in}}\left(n_i f_n - n_n f_i\right) - R_{\text{ion}} n_e f_n, \tag{2}$$

$$n_s(z,t) = \int_{-\infty}^{\infty} dv_\parallel f_s(z, v_\parallel, t), \tag{3}$$

and

$$n_i = n_e = N_e \exp\left(\frac{e\phi}{T_e}\right), \tag{4}$$

with $f_s \doteq \int d\vartheta dv_\perp v_\perp F_s$ the marginalized particle distribution function for species $s$, $v_\parallel$ and $v_\perp$ the components of the particle velocity parallel and perpendicular to the magnetic field, respectively, $\vartheta$ the gyro-angle, $t$ the time, $\phi$ the electrostatic potential, and $R_{\text{in}}$ and $R_{\text{ion}}$ charge exchange and ionization collision frequency factors.

## 3. Moment kinetics

One can separately evolve velocity space moments of the particle distribution function (pdf) via judicious choices for the parallel velocity coordinate and for the normalisation of the evolved pdf. This approach presents a number of potential advantages: the use of fluid equations for low-order moments of $f$ could be useful in formulating a scheme that switches between fluid and kinetic treatments where appropriate (and possibly also between small and large amplitude fluctuations of $f$); separate evolution of an electron momentum equation should allow for an explicit equation for the electrostatic potential, which otherwise must be solved implicitly or via an iterative solver; conservation properties for the low-order moments may be easier to enforce; and use of a velocity coordinate normalised by the local thermal speed should be more efficient than the use of a coordinate normalised by some global speed. To our knowledge, this 'moment kinetic' approach has not been attempted before, and the aim of this report is to identify any

challenges faced by this approach and to present solutions to these challenges where possible.

We have considered four variations of the moment kinetic approach corresponding to different combinations of the particle density, parallel flow and parallel pressure being evolved separately from an appropriately normalised pdf. In the following sub-sections we present the system of equations used for each of these moment kinetic models.

### *3.1. Density evolution*

In this subsection, we describe a moment-kinetic model in which the particle density is evolved separately from an appropriately normalised particle distribution function. To separate the evolution of the particle density from that of the particle distribution function, we define the normalised distribution function

$$g_s \doteq \frac{f_s}{n_s}. \tag{5}$$

The zeroth velocity moment of $g_s$ satisfies

$$\int dv_\parallel g_s = 1, \tag{6}$$

and the kinetic equations for $g_\mathrm{i}$ and $g_n$, obtained by substituting Eq. 5 into Eqs. (1) and (2), are

$$n_i\frac{\partial g_i}{\partial t} + g_i\frac{\partial n_i}{\partial t} + v_\parallel\frac{\partial f_i}{\partial z} - \frac{en_i}{m_i}\frac{\partial\phi}{\partial z}\frac{\partial g_i}{\partial v_\parallel} = -R_\mathrm{in}n_in_n\left(g_i - g_n\right) + R_\mathrm{ion}n_\mathrm{i}n_ng_n, \tag{7}$$

and

$$n_n\frac{\partial g_n}{\partial t} + g_n\frac{\partial n_n}{\partial t} + v_\parallel\frac{\partial f_n}{\partial z} = -R_\mathrm{in}n_in_n\left(g_n - g_i\right) - R_\mathrm{ion}n_\mathrm{i}n_ng_n, \tag{8}$$

respectively.

Taking the $v_\parallel$ moment of the kinetic equations (1) and (2) results in the continuity equation that describes the time evolution of the ion and neutral densities:

$$\frac{\partial n_s}{\partial t} + \frac{\partial n_su_s}{\partial z} = \pm R_\mathrm{ion}n_in_n, \tag{9}$$

with the plus and minus signs corresponding to the ion and neutral density evolution equations, respectively. Substituting Eq. (9) into Eqs. (7) and (8) eliminates the time derivatives of the density, leaving

$$\frac{\partial g_i}{\partial t} + \frac{v_\parallel}{n_i}\frac{\partial f_i}{\partial z} - \frac{e}{m_i}\frac{\partial\phi}{\partial z}\frac{\partial g_i}{\partial v_\parallel} = \frac{g_i}{n_i}\frac{\partial n_\mathrm{i}u_\mathrm{i}}{\partial z} + \left(R_\mathrm{in} + R_\mathrm{ion}\right)n_n\left(g_n - g_\mathrm{i}\right), \tag{10}$$

and

$$\frac{\partial g_n}{\partial t} + \frac{v_\parallel}{n_n}\frac{\partial f_n}{\partial z} = \frac{g_n}{n_n}\frac{\partial n_nu_n}{\partial z} - R_\mathrm{in}n_i\left(g_n - g_i\right). \tag{11}$$

Eqs. (9)-(11), along with the assumed Boltzmann response given by Eq. (4) and the relation (5) between $f$ and $g$, constitute a closed system of equations for the evolved quantities $\{g_i, g_n, n_i, n_n\}$. Boundary conditions must be specified to ensure a unique solution, and this will be discussed in Sec. 4.

### *3.2. Density and parallel flow evolution*

In this subsection, we describe a moment-kinetic model in which both the particle density and parallel flow are evolved separately from an appropriately normalised particle distribution function. To separate the evolution of both the particle density and the parallel flow from that of the particle distribution function, we again define the normalised distribution function

$$g_s(z, w_\parallel, t) \doteq \frac{f_s(z, w_\parallel, t)}{n_s(z,t)}, \tag{12}$$

which is now a function of the peculiar velocity $w_\parallel \doteq v_\parallel - u_s$, with the parallel flow defined via

$$n_s u_s \doteq \int dv_\parallel v_\parallel f_s. \tag{13}$$

The zeroth and first velocity moments of $g_s$ satisify

$$\int dw_\parallel g_s = 1 \tag{14}$$

and

$$\int dw_\parallel w_\parallel g_s = 0. \tag{15}$$

The kinetic equation for $g_s$, obtained by substituting Eq. (12) into Eqs. (1) and (2), is

$$\frac{\partial g_s}{\partial t} + \frac{g_s}{n_s}\frac{\partial n_s}{\partial t} + \frac{\left(w_\parallel + u_s\right)}{n_s}\frac{\partial f_s}{\partial z} + \dot{w}_{\parallel,s}\frac{\partial g_s}{\partial w_\parallel} = -R_{\mathrm{ss'}} n_{s'}\left(g_s - g_{s'}\right) \pm R_{\mathrm{ion}} n_{s'} g_n, \tag{16}$$

where $\{s, s'\} = \{i, n\}$ or $\{s, s'\} = \{n, i\}$, the $+$ $(-)$ sign corresponds to ions (neutrals), the $z$ and $t$ derivatives are taken at fixed $w_\parallel$, the effective parallel acceleration for species $s$ is

$$\dot{w}_{\parallel,s} \doteq -\left(\delta_{s,i}\frac{e}{m_i}\frac{\partial \phi}{\partial z} + \frac{\partial u_s}{\partial t} + \left(w_\parallel + u_s\right)\frac{\partial u_s}{\partial z}\right), \tag{17}$$

and we have used

$$\frac{\partial}{\partial v_\parallel} = \frac{\partial}{\partial w_\parallel}, \tag{18}$$

$$\left.\frac{\partial}{\partial t}\right|_{v_\parallel} = \left.\frac{\partial}{\partial t}\right|_{w_\parallel} + \left.\frac{\partial w_\parallel}{\partial t}\right|_{v_\parallel}\frac{\partial}{\partial w_\parallel} = \left.\frac{\partial}{\partial t}\right|_{w_\parallel} - \frac{\partial u_s}{\partial t}\frac{\partial}{\partial w_\parallel} \tag{19}$$

and

$$\left.\frac{\partial}{\partial z}\right|_{v_\parallel} = \left.\frac{\partial}{\partial z}\right|_{w_\parallel} + \left.\frac{\partial w_\parallel}{\partial z}\right|_{v_\parallel}\frac{\partial}{\partial w_\parallel} = \left.\frac{\partial}{\partial z}\right|_{w_\parallel} - \frac{\partial u_s}{\partial z}\frac{\partial}{\partial w_\parallel}. \tag{20}$$

The continuity equation (9) is used to evolve the particle density, and the parallel momentum equation – obtained by multiplying the kinetic equations (1) and (2) by $m_s v_\parallel$ and integrating over all $v_\parallel$ – is now needed to evolve $u_s$:

$$\frac{\partial\left(m_s n_s u_s\right)}{\partial t} = -\frac{\partial\left(p_{\parallel,s} + m_s n_s u_s^2\right)}{\partial z} - \delta_{s,i} e n_s \frac{\partial \phi}{\partial z} + m_s R_{ss'} n_s n_{s'}\left(u_{s'} - u_s\right) \pm m_s R_{\mathrm{ion}} n_s n_{s'} u_n, \tag{21}$$

where the parallel pressure $p_{\parallel,s}$ is defined as

$$p_{\parallel,s} \doteq \int_{-\infty}^{\infty} m_s w_\parallel^2 f_s. \tag{22}$$

The time derivative of $u_s$ appearing in Eq. (17) can be re-expressed using the parallel momentum equation (21) and the continuity equation (9):

$$\frac{\partial u_s}{\partial t} = \frac{u_s}{n_s}\frac{\partial n_s u_s}{\partial z} - \frac{1}{m_s n_s}\frac{\partial\left(p_{\parallel,s} + m_s n_s u_s^2\right)}{\partial z} + \left(R_{ss'} + \delta_{s,i}R_{\text{ion}}\right) n_{s'}\left(u_{s'} - u_s\right) - \delta_{s,i}\frac{e}{m_s}\frac{\partial\phi}{\partial z}. \tag{23}$$

Substituting the above expression into the parallel acceleration equation (17) yields

$$\dot{w}_{\parallel,s} = \frac{1}{m_s n_s}\frac{\partial p_{\parallel,s}}{\partial z} - \left(R_{\text{in}} + \delta_{s,i}R_{\text{ion}}\right) n_{s'}\left(u_{s'} - u_s\right) - w_\parallel\frac{\partial u_s}{\partial z}. \tag{24}$$

Finally, we eliminate the time derivative of the density appearing in Eq. (16) by using the continuity equation (9), giving

$$\frac{\partial g_s}{\partial t} + \frac{\left(w_\parallel + u_s\right)}{n_s}\frac{\partial f_s}{\partial z} + \dot{w}_{\parallel,s}\frac{\partial g_s}{\partial w_\parallel} = g_s\frac{\partial n_s u_s}{\partial z} + \left(R_{\text{in}} + \delta_{s,i}R_{\text{ion}}\right) n_{s'}\left(g_{s'} - g_s\right). \tag{25}$$

Subject to the specification of boundary conditions in Sec. 4, Eqs. (9), (21), (24) and (25), along with the assumed Boltzmann response given by Eq. (4) and the relation (12) between $f$ and $g$, constitute a closed system of equations for the evolved quantities $\{g_i, g_n, n_i, n_n, u_i, u_n\}$.

### *3.3. Density and parallel pressure evolution*

In this subsection, we describe a moment-kinetic model in which both the particle density and parallel pressure are evolved separately from an appropriately normalised particle distribution function. To separate the evolution of both the particle density and the parallel pressure from that of the particle distribution function $f$, we define the normalised distribution function

$$\hat{g}_s(z, \hat{v}_\parallel, t) \doteq f_s(z, \hat{v}_\parallel, t)\frac{v_{\text{th},s}(z,t)}{n_s(z,t)}, \tag{26}$$

where the normalised parallel velocity is

$$\hat{v}_\parallel \doteq \frac{v_\parallel}{v_{\text{th},s}}, \tag{27}$$

the thermal speed is

$$v_{\text{th},s} \doteq \sqrt{\frac{2T_{\parallel,s}}{m_s}}, \tag{28}$$

the parallel pressure and temperature are

$$\begin{aligned} p_{\parallel,s} \doteq n_s T_{\parallel,s} &= \int dv_\parallel m_s w_\parallel^2 f_s \\ &= 2p_{\parallel,s} \int d\hat{v}_\parallel \left( \hat{v}_\parallel^2 - \frac{u_s^2}{v_{\mathrm{th},s}^2} \right) \hat{g}_s, \end{aligned} \tag{29}$$

the peculiar parallel velocity is $w_\parallel = v_\parallel - u_s$, and the parallel flow is

$$u_s \doteq \frac{1}{n_s} \int dv_\parallel v_\parallel f_s = v_{\mathrm{th},s} \int d\hat{v}_\parallel \hat{v}_\parallel \hat{g}_s. \tag{30}$$

The zeroth, first and second velocity moments of $\hat{g}_s$ satisify

$$\int d\hat{v}_\parallel \hat{g}_s = 1, \tag{31}$$

$$\int d\hat{v}_\parallel \hat{v}_\parallel \hat{g}_s = \frac{u_s}{v_{\mathrm{th},s}} \tag{32}$$

and

$$\int d\hat{v}_\parallel \hat{v}_\parallel^2 \hat{g}_s = \frac{1}{2} + \frac{u_s^2}{v_{\mathrm{th},s}^2}. \tag{33}$$

The kinetic equation for $\hat{g}_s$, obtained by substituting Eq. (26) into Eqs. (1) and (2), is

$$\begin{aligned} &\frac{\partial \hat{g}_s}{\partial t} + \hat{g}_s \left( \frac{\partial \ln n_s}{\partial t} - \frac{\partial \ln v_{\mathrm{th},s}}{\partial t} \right) + \frac{v_{\mathrm{th},s}^2}{n_s} \hat{v}_\parallel \frac{\partial f_s}{\partial z} + \dot{\hat{v}}_{\parallel,s} \frac{\partial \hat{g}_s}{\partial \hat{v}_\parallel} \\ &\quad = -R_{ss'} n_{s'} \left( \hat{g}_s - \hat{g}_{s'} \frac{v_{\mathrm{th},s}}{v_{\mathrm{th},s'}} \right) \pm R_{\mathrm{ion}} \hat{g}_n n_{s'} \frac{v_{\mathrm{th},s}}{v_{\mathrm{th},n}}, \end{aligned} \tag{34}$$

where $\{s, s'\} = \{i, n\}$ or $\{s, s'\} = \{n, i\}$, the $+$ $(-)$ sign corresponds to ions (neutrals), the $z$ and $t$ derivatives are taken at fixed $\hat{v}_\parallel$, the effective parallel acceleration for species $s$ is

$$\dot{\hat{v}}_{\parallel,s} \doteq - \left( \delta_{s,i} \frac{e}{m_s v_{\mathrm{th},s}} \frac{\partial \phi}{\partial z} + \hat{v}_\parallel \frac{\partial \ln v_{\mathrm{th},s}}{\partial t} + v_{\mathrm{th},s} \hat{v}_\parallel^2 \frac{\partial \ln v_{\mathrm{th},s}}{\partial z} \right), \tag{35}$$

and we have used

$$\frac{\partial}{\partial v_\parallel} = \frac{1}{v_{\mathrm{th},s}} \frac{\partial}{\partial \hat{v}_\parallel}, \tag{36}$$

$$\left. \frac{\partial}{\partial t} \right|_{v_\parallel} = \left. \frac{\partial}{\partial t} \right|_{\hat{v}_\parallel} + \left. \frac{\partial \hat{v}_\parallel}{\partial t} \right|_{v_\parallel} \frac{\partial}{\partial \hat{v}_\parallel} = \left. \frac{\partial}{\partial t} \right|_{\hat{v}_\parallel} - \hat{v}_\parallel \frac{\partial \ln v_{\mathrm{th},s}}{\partial t} \frac{\partial}{\partial \hat{v}_\parallel} \tag{37}$$

and

$$\left. \frac{\partial}{\partial z} \right|_{v_\parallel} = \left. \frac{\partial}{\partial z} \right|_{\hat{v}_\parallel} + \left. \frac{\partial \hat{v}_\parallel}{\partial z} \right|_{v_\parallel} \frac{\partial}{\partial \hat{v}_\parallel} = \left. \frac{\partial}{\partial z} \right|_{\hat{v}_\parallel} - \hat{v}_\parallel \frac{\partial \ln v_{\mathrm{th},s}}{\partial z} \frac{\partial}{\partial \hat{v}_\parallel}. \tag{38}$$

The continuity equation (9) is used to evolve the particle density, and the parallel energy equation – obtained by multiplying the kinetic equations (1) and (2) by $m_s w_\parallel^2$

and integrating over all $w_\parallel$ – is now needed to evolve $p_{\parallel,s}$:

$$\begin{aligned}\frac{\partial p_{\parallel,s}}{\partial t}+u_s\frac{\partial p_{\parallel,s}}{\partial z} &= m_s n_s v_{\mathrm{th},s}\left(\frac{\partial v_{\mathrm{th},s}}{\partial t}+u_s\frac{\partial v_{\mathrm{th},s}}{\partial z}\right)+T_{\parallel,s}\left(\frac{\partial n_s}{\partial t}+u_s\frac{\partial n_s}{\partial z}\right)\\ &= -\frac{\partial q_{\parallel,s}}{\partial z}-3p_{\parallel,s}\frac{\partial u_s}{\partial z}-R_{\mathrm{ss'}}\left(n_{s'}p_{\parallel,s}-n_s p_{\parallel,s'}\right)\pm R_{\mathrm{ion}}n_e p_{\parallel,n},\end{aligned} \tag{39}$$

where we have defined the parallel heat flux

$$\begin{aligned}q_{\parallel,s} &\doteq \int dv_\parallel m_s w_\parallel^3 f_s\\ &= m_s n_s v_{\mathrm{th},s}^3\int d\hat{v}_\parallel\left(\hat{v}_\parallel-\frac{u_s}{v_{\mathrm{th},s}}\right)^3\hat{g}_s.\end{aligned} \tag{40}$$

The time derivatives of $v_{\mathrm{th},s}$ appearing in Eqs. (34) and (35) can be re-expressed using the energy equation (39) and the continuity equation (9):

$$\frac{\partial \ln v_{\mathrm{th},s}}{\partial t}=\frac{R_{\mathrm{ss'}}}{2}n_{s'}\left(\frac{T_{\parallel,s'}}{T_{\parallel,s}}-1\right)-\frac{1}{v_{\mathrm{th},s}}\frac{\partial u_s v_{\mathrm{th},s}}{\partial z}\pm\frac{R_{\mathrm{ion}}}{2}n_{s'}\left(\frac{T_{\parallel,n}}{T_{\parallel,s}}-1\right)-\frac{1}{2p_{\parallel,s}}\frac{\partial q_{\parallel,s}}{\partial z}. \tag{41}$$

Substituting this expression into the parallel acceleration expression (35) gives

$$\begin{aligned}\dot{\hat{v}}_{\parallel,s} = &-\left(\delta_{s,i}\frac{e}{m_s v_{\mathrm{th},s}}\frac{\partial\phi}{\partial z}+v_{\mathrm{th},s}\hat{v}_\parallel^2\frac{\partial\ln v_{\mathrm{th},s}}{\partial z}\right)\\ &+\hat{v}_\parallel\left(\left(R_{ss'}+\delta_{s,i}R_{\mathrm{ion}}\right)\frac{n_{s'}}{2}\left(1-\frac{T_{\parallel,s'}}{T_{\parallel,s}}\right)+\frac{1}{v_{\mathrm{th},s}}\frac{\partial u_s v_{\mathrm{th},s}}{\partial z}+\frac{1}{2p_{\parallel,s}}\frac{\partial q_{\parallel,s}}{\partial z}\right).\end{aligned} \tag{42}$$

Finally, we substitute Eqs. (9) and (41) into the kinetic equation (34) to find

$$\begin{aligned}\frac{\partial\hat{g}_s}{\partial t}+\frac{v_{\mathrm{th},s}^2}{n_s}\hat{v}_\parallel\frac{\partial f_s}{\partial z}+\dot{\hat{v}}_{\parallel,s}\frac{\partial\hat{g}_s}{\partial\hat{v}_\parallel} &= \hat{g}_s u_s\left(\frac{\partial\ln n_s}{\partial z}-\frac{\partial\ln v_{\mathrm{th},s}}{\partial z}\right)-\frac{\hat{g}_s}{2p_{\parallel,s}}\frac{\partial q_{\parallel,s}}{\partial z}\\ &-\left(R_{ss'}+\delta_{s,i}R_{\mathrm{ion}}\right)n_{s'}\left(\hat{g}_s-\hat{g}_{s'}\frac{v_{\mathrm{th},s}}{v_{\mathrm{th},s'}}\right)+\hat{g}_s\left(\frac{n_{s'}}{2}\left(R_{ss'}+\delta_{s,i}R_{\mathrm{ion}}\right)\left(\frac{T_{\parallel,s'}}{T_{\parallel,s}}-1\right)\right).\end{aligned} \tag{43}$$

Subject to the specification of boundary conditions in Sec. 4, Eqs. (9), (35), (39) and (43), along with the assumed Boltzmann response given by Eq. (4) and the relation (26) between $f$ and $g$, constitute a closed system of equations for the evolved quantities $\{\hat{g}_i, \hat{g}_n, n_i, n_n, p_{\parallel,i}, p_{\parallel,n}\}$.

### *3.4. Density, parallel flow and parallel pressure evolution*

In this subsection, we describe a moment-kinetic model in which the particle density, parallel flow and parallel pressure are all evolved separately from an appropriately normalised particle distribution function. To separate the evolution of these low-order moments from that of the particle distribution function $f$, we again define the normalised distribution function

$$\hat{g}_s(z,\hat{w}_\parallel,t)\doteq f_s(z,\hat{w}_\parallel,t)\frac{v_{\mathrm{th},s}(z,t)}{n_s(z,t)}, \tag{44}$$

where $\hat{g}_s$ is now a function of the normalised peculiar velocity

$$\hat{w}_\parallel \doteq \frac{v_\parallel - u_s}{v_{\mathrm{th},s}}. \tag{45}$$

With these definitions, the lowest three moments of $\hat{g}_s$ satisfy

$$\int d\hat{w}_\parallel \left(1, \hat{w}_\parallel, \hat{w}_\parallel^2\right) \hat{g}_s = \left(1, 0, \frac{1}{2}\right). \tag{46}$$

The kinetic equation for $\hat{g}_s$, obtained by substituting Eq. (44) into Eqs. (1) and (2), is identical in form to Eq. (43):

$$\begin{aligned}\frac{\partial \hat{g}_s}{\partial t} + \frac{v_{\mathrm{th},s}}{n_s}\left(v_{\mathrm{th},s}\hat{w}_\parallel + u_s\right)\frac{\partial f_s}{\partial z} + \dot{\hat{w}}_{\parallel,s}\frac{\partial \hat{g}_s}{\partial \hat{w}_\parallel} = \hat{g}_s u_s\left(\frac{\partial \ln n_s}{\partial z} - \frac{\partial \ln v_{\mathrm{th},s}}{\partial z}\right) - \frac{\hat{g}_s}{2p_{\parallel,s}}\frac{\partial q_{\parallel,s}}{\partial z} \\ - \left(R_{ss'} + \delta_{s,i}R_{\mathrm{ion}}\right) n_{s'}\left(\hat{g}_s - \hat{g}_{s'}\frac{v_{\mathrm{th},s}}{v_{\mathrm{th},s'}}\right) + \hat{g}_s\left(\frac{n_{s'}}{2}\left(R_{ss'} + \delta_{s,i}R_{\mathrm{ion}}\right)\left(\frac{T_{\parallel,s'}}{T_{\parallel,s}} - 1\right)\right),\end{aligned} \tag{47}$$

where $\{s, s'\} = \{i, n\}$ or $\{s, s'\} = \{n, i\}$, the $z$ and $t$ derivatives are taken at fixed $\hat{w}_\parallel$, the effective parallel acceleration for species $s$ is

$$\begin{aligned}\dot{\hat{w}}_{\parallel,s} = &- \hat{w}_\parallel^2\frac{\partial v_{\mathrm{th},s}}{\partial z} + \frac{1}{v_{\mathrm{th},s}}\left(\frac{1}{m_s n_s}\frac{\partial p_{\parallel,s}}{\partial z} - R_{\mathrm{ss'}}n_{s'}\left(u_{s'} - u_s\right) \mp R_{\mathrm{ion}}n_{s'}\left(u_n - u_s\right)\right) \\ &+ \hat{w}_\parallel\left(\frac{1}{2p_{\parallel,s}}\frac{\partial q_{\parallel,s}}{\partial z} + \left(R_{\mathrm{ss'}} + \delta_{s,i}R_{\mathrm{ion}}\right)\frac{n_{s'}}{2}\left(1 - \frac{T_{\parallel,s'}}{T_{\parallel,s}}\right)\right),\end{aligned} \tag{48}$$

with the top and bottom signs in Eq. (48) corresponding to ions and neutrals, respectively, and we have used

$$\frac{\partial}{\partial v_\parallel} = \frac{1}{v_{\mathrm{th},s}}\frac{\partial}{\partial \hat{w}_\parallel}, \tag{49}$$

$$\left.\frac{\partial}{\partial t}\right|_{v_\parallel} = \left.\frac{\partial}{\partial t}\right|_{\hat{w}_\parallel} + \left.\frac{\partial \hat{w}_\parallel}{\partial t}\right|_{v_\parallel}\frac{\partial}{\partial \hat{w}_\parallel} = \left.\frac{\partial}{\partial t}\right|_{\hat{w}_\parallel} - \left(\frac{1}{v_{\mathrm{th},s}}\frac{\partial u_s}{\partial t} + \hat{w}_\parallel\frac{\partial \ln v_{\mathrm{th},s}}{\partial t}\right)\frac{\partial}{\partial \hat{w}_\parallel} \tag{50}$$

and

$$\left.\frac{\partial}{\partial z}\right|_{v_\parallel} = \left.\frac{\partial}{\partial z}\right|_{\hat{w}_\parallel} + \left.\frac{\partial \hat{w}_\parallel}{\partial z}\right|_{v_\parallel}\frac{\partial}{\partial \hat{w}_\parallel} = \left.\frac{\partial}{\partial z}\right|_{\hat{w}_\parallel} - \left(\frac{1}{v_{\mathrm{th},s}}\frac{\partial u_s}{\partial z} + \hat{w}_\parallel\frac{\partial \ln v_{\mathrm{th},s}}{\partial z}\right)\frac{\partial}{\partial \hat{w}_\parallel}. \tag{51}$$

Subject to the specification of boundary conditions in Sec. 4, Eqs. (9), (21), (39), (47) and (48), along with the assumed Boltzmann response given by Eq. (4) and the relation (44) between $f$ and $g$, constitute a closed system of equations for the evolved quantities $\{\hat{g}_i, \hat{g}_n, n_i, n_n, u_i, u_n, p_{\parallel,i}, p_{\parallel,n}\}$.

## 4. Boundary conditions

To ensure that the solutions to the model equations described in Secs. 2 and 3 are unique, we must specify boundary conditions for the evolved particle distribution function in $z$ and in the parallel velocity coordinate. The physical boundary condition in $v_\parallel$ is that $f_s(z, v_\parallel \to \pm\infty, t) \to 0$. This translates with little difficulty to the normalised pdfs $g_s$ and $\hat{g}_s$, regardless of the choice of parallel velocity coordinate. One may also enforce that $f_s$ is periodic in $v_\parallel$ at the extremes of the $v_\parallel$ domain, which will be equivalent to the zero boundary condition above if the $v_\parallel$ domain is sufficiently large.

As for the boundary condition in $z$, there are (at least) two options that are physically interesting: periodic boundary conditions and so-called 'wall' boundary conditions. The former are applicable for plasma streaming along magnetic field lines that are closed, either mapping out a line or a toroidal surface. Those field lines that form a closed line are physically periodic, while those ergodically mapping out a toroidal surface give rise to dynamics that are periodic in a statistical sense. Wall boundary conditions are needed when considering 'open' field lines that terminate at the vessel wall. Here we describe the wall boundary conditions that we impose on our model equations.

Complicated dynamics occur close to the wall, leading to a hierarchy of narrow layers with different dynamics. Derivation of the equations that describe these 'sheaths' is an ongoing research activity in the magnetic confinement fusion community. We avoid such complications here by considering a plasma domain whose boundaries in $z$ are the entrances to the sheaths furthest from the wall.

Ions that exit the simulation domain are assumed to continue on to the wall, where they recombine. As a result, no ions enter the domain from the walls, giving a zero incoming BC for the ions:

$$F_i(z = 0, v_\parallel > 0, v_\perp, t) = 0 = F_i(z = L_z, v_\parallel < 0, v_\perp, t), \tag{52}$$

where $F$ is the un-marginalised particle distribution function, and the boundaries of our domain (corresponding to the sheath entrances) are taken to be at $z = 0$ and $z = L_z$. Neutrals that leave the domain are assumed to hit the wall and thermalise at the temperature of the wall, $T_w$. Ions that recombine at the wall also re-enter as neutrals. The resulting boundary condition on the neutrals is

$$F_n(z = 0, v_\parallel > 0, v_\perp, t) = \Gamma_0 F_{Kw}(v_\parallel, v_\perp), \quad F_n(z = L_z, v_\parallel < 0, v_\perp, t) = \Gamma_{L_z} F_{Kw}(v_\parallel, v_\perp), \tag{53}$$

where

$$F_{Kw}(v_\parallel, v_\perp) \doteq \frac{3}{\pi}\left(\frac{m_i}{2T_w}\right)^2 \frac{\left|v_\parallel\right|}{\sqrt{v_\parallel^2 + v_\perp^2}} \exp\left(-\frac{m_i\left(v_\parallel^2 + v_\perp^2\right)}{2T_w}\right) \tag{54}$$

is the Knudsen cosine distribution, and

$$\Gamma_0 \doteq \sum_{s=i,n} 2\pi \int_{-\infty}^{0} dv_\parallel \int_0^\infty dv_\perp v_\perp \left|v_\parallel\right| F_s(z = 0, v_\parallel, v_\perp, t) \tag{55}$$

and

$$\Gamma_{L_z} \doteq \sum_{s=i,n} 2\pi \int_0^\infty dv_\parallel \int_0^\infty dv_\perp v_\perp \left|v_\parallel\right| F_s(z=L_z, v_\parallel, v_\perp, t) \tag{56}$$

are the combined fluxes of neutrals and ions towards the walls at $z = 0$ and $z = L_z$, respectively.

We next marginalise the above distribution functions by integrating over gyro-angle and $v_\perp$ to get

$$f_i(z=0, v_\parallel > 0, t) = 0 = f_i(z=L_z, v_\parallel < 0, t) \tag{57}$$

and

$$f_n(z=0, v_\parallel > 0, t) = \Gamma_0 f_{Kw}(v_\parallel), \quad f_n(z=L_z, v_\parallel < 0, t) = \Gamma_{L_z} f_{Kw}(v_\parallel), \tag{58}$$

with

$$f_{Kw}(v_\parallel) \doteq 2\pi \int_0^\infty dv_\perp v_\perp F_{Kw}(v_\parallel, v_\perp) = 3\sqrt{\pi} \left(\frac{m_i}{2T_w}\right)^{3/2} \left|v_\parallel\right| \operatorname{erfc}\left(\sqrt{\frac{m_i}{2T_w}} \left|v_\parallel\right|\right) \tag{59}$$

and erfc the complementary error function. The fluxes toward the wall at the domain boundaries can be recast in terms of the marginalised distribution function:

$$\Gamma_0 = \sum_{s=i,n} \int_{-\infty}^0 dv_\parallel \left|v_\parallel\right| f_s(z=0, v_\parallel, t) \tag{60}$$

and

$$\Gamma_{L_z} = \sum_{s=i,n} \int_0^\infty dv_\parallel \left|v_\parallel\right| f_s(z=L_z, v_\parallel, t). \tag{61}$$

It is worth considering the constraint imposed by these boundary conditions on the evolution of the line-averaged species densities, $\langle n_s \rangle$. Taking the $z$ average of the continuity equation (9), we obtain

$$\frac{\partial \langle n_s \rangle}{\partial t} = \frac{1}{L_z} \left(\Gamma_s(z=0) - \Gamma_s(z=L_z)\right) \pm R_{\text{ion}} \langle n_i n_n \rangle , \tag{62}$$

with $\langle A \rangle = (\int dz A)/L_z$, and the + and - signs corresponding to ions and to neutrals, respectively. For the ions

$$\Gamma_i(0) = \int_{-\infty}^0 dv_\parallel v_\parallel f_i(z=0, v_\parallel) < 0, \tag{63}$$

and

$$\Gamma_i(L_z) = \int_0^\infty dv_\parallel v_\parallel f_i(z=L_z, v_\parallel) > 0, \tag{64}$$

where we have used the boundary conditions on $f_i$ given by expression (57).

For the neutrals

$$\begin{aligned} \Gamma_n(0) &= \int_{-\infty}^0 dv_\parallel v_\parallel f_n(z=0, v_\parallel) + \Gamma_0 \int_0^\infty dv_\parallel v_\parallel f_{Kw}(v_\parallel) \\ &= \int_{-\infty}^0 dv_\parallel v_\parallel f_n(z=0, v_\parallel) + \Gamma_0, \end{aligned} \tag{65}$$

and

$$\begin{aligned}\Gamma_n(L_z) &= \int_0^\infty dv_\parallel v_\parallel f_n(z=L_z,v_\parallel) + \Gamma_{L_z}\int_{-\infty}^0 dv_\parallel v_\parallel f_{Kw}(v_\parallel) \\ &= \int_0^\infty dv_\parallel v_\parallel f_n(z=L_z,v_\parallel) - \Gamma_{L_z},\end{aligned} \tag{66}$$

where we have used the boundary conditions on $f_n$ given by expression (58) and the fact that $\int_0^\infty dv_\parallel v_\parallel f_{Kw} = -\int_{-\infty}^0 dv_\parallel v_\parallel f_{Kw} = 1$.

Combining the results for the ion and neutral densities and noting that the ionization contributions to the ion and neutral densities cancel, we obtain a constraint on the evolution of the total (species-summed), line-averaged density:

$$\begin{aligned}\frac{\partial}{\partial t}\sum_{s=i,n}\langle n_s\rangle &= \frac{1}{L_z}\sum_{s=i,n}\left(\Gamma_s(z=0)-\Gamma_s(z=L_z)\right) \\ &= \frac{1}{L_z}\left(\sum_{s=i,n}\int_{-\infty}^0 v_\parallel f_s(z=0,v_\parallel)+\Gamma_0-\sum_{s=i,n}\int_0^\infty v_\parallel f_s(z=L_z,v_\parallel)+\Gamma_{L_z}\right) \\ &= 0.\end{aligned} \tag{67}$$

This is a consequence of the assumed wall boundary condition, which dictates that any particles leaving the domain re-enter as neutrals (and thus total density is conserved). It can be used to test the numerical implementation of the wall boundary condition, discussed in Sec. 6.

In the following sub-sections, we re-cast these wall boundary conditions in terms of the normalised distribution functions and modified velocity coordinates described in Secs. 2 and 3.

### *4.1. Analytical solution in simplified limit*

We can derive an analytical solution for the electrostatic potential for our system by neglecting charge exchange collisions and by replacing the ionisation source term appearing in Eq. (1) with a simplified source. In particular, we follow the approach of Ref. [6] and assume that ionisation occurs at a constant rate and gives birth to ions with zero parallel velocity. The resulting ion kinetic equation is

$$\frac{\partial f_i}{\partial t} + v_\parallel\frac{\partial f_i}{\partial z} - \frac{e}{m_i}\frac{\partial\phi}{\partial z}\frac{\partial f_i}{\partial v_\parallel} = R_{\text{ion}}N_e^2\delta(v_\parallel), \tag{68}$$

with $\delta(v_\parallel)$ the Dirac delta distribution. With these assumptions, the ion kinetic equation decouples from the kinetic equation for the neutrals and makes the problem tractable.

Ions that are formed at a given spatial location $z_0$ are accelerated toward the walls by the parallel electric field set up by the wall boundary condition. The parallel speed

of these ions after travelling to a location $z$ that is closer to the wall, $v_\parallel(z)$, is obtained via conservation of energy:

$$\frac{m_i v_\parallel(z)^2}{2} = e\left(\phi(z_0) - \phi(z)\right). \tag{69}$$

In steady-state, the flux of ions with speeds in the range $v_\parallel$ to $v_\parallel + dv_\parallel$ through the location $z$ must equal the rate at which these ions are generated between $z_0$ and $z_0 + dz_0$:

$$v_\parallel(z) f_i(v_\parallel(z)) dv_\parallel = N_e^2 R_{\text{ion}} dz_0. \tag{70}$$

Combining Eqs. (69) and (70) and imposing quasineutrality gives

$$\begin{aligned} N_e \exp\left(\frac{e\phi(z)}{T_e}\right) = \int dv_\parallel f_i(z, v_\parallel) &= \int_z^{L_z/2} \sqrt{\frac{m_i}{2e}} \frac{N_e^2 R_{\text{ion}}}{\sqrt{\phi(z_0) - \phi(z)}} dz_0 \\ &= \int_{\phi(z)}^{\phi(L_z/2)} \sqrt{\frac{m_i}{2e}} \frac{N_e^2 R_{\text{ion}}}{\sqrt{\phi(z_0) - \phi(z)}} \frac{dz_0}{d\phi(z_0)} d\phi(z_0), \end{aligned} \tag{71}$$

which is an implicit equation for $\phi(z)$. Setting our gauge so that $\phi(L_z/2) = 0$, and defining $x \doteq -e\phi(z_0)/T_e$ and $y \doteq -e\phi(z)/T_e$, we have

$$N_e \exp(-y) = \int_0^y \frac{h(x)}{\sqrt{y - x}} dx, \tag{72}$$

where

$$h(x) \doteq \frac{N_e^2 R_{\text{ion}}}{c_s} \frac{dz_0}{dx}. \tag{73}$$

The density integral appearing in Eq. (72) is of the form of an Abel transform [7], which can be inverted to yield

$$h(x) = \frac{N_e}{\pi} \frac{d}{dx} \int_0^x dy \frac{\exp(-y)}{\sqrt{x - y}}. \tag{74}$$

Equating (73) and (74) yields an expression for $dz/dx$:

$$\frac{dz}{dx} = \frac{c_s}{N_e R_{\text{ion}} \pi} \frac{d}{dx} \int_0^x dy \frac{\exp(-y)}{\sqrt{x - y}}. \tag{75}$$

Integrating with respect to $x$ yields an implicit expression for $\phi(z)$:

$$\begin{aligned} z - \frac{L_z}{2} &= \pm \frac{c_s}{\pi R_{\text{ion}} N_e} \int_0^x dy \frac{\exp(-y)}{\sqrt{x - y}} \\ &= \pm \frac{2c_s}{\pi R_{\text{ion}} N_e} D\left(\sqrt{-\frac{e\phi(z)}{T_e}}\right), \end{aligned} \tag{76}$$

with $D(a) = \exp(-a^2) \int_0^a \exp(b^2) db$ the Dawson function, the $+$ sign corresponds to $z > L_z/2$ and the $-$ sign corresponds to $z < L_z/2$.

*4.2. Density evolution*

We consider the wall boundary conditions in terms of the modified distribution function $g_s$ given in Eq. (5). The boundary conditions on the ions and neutrals are

$$g_i(z=0, v_\parallel > 0, t) = 0 = g_i(z=L_z, v_\parallel < 0, t) \tag{77}$$

and

$$\begin{aligned} g_n(z=0, v_\parallel > 0, t) &= \frac{\Gamma_0}{n_n} f_{Kw}(v_\parallel), \\ g_n(z=L_z, v_\parallel < 0, t) &= \frac{\Gamma_{L_z}}{n_n} f_{Kw}(v_\parallel), \end{aligned} \tag{78}$$

with the Knudsen cosine distribution given by Eq. (59) and the fluxes toward the wall at the domain boundaries

$$\Gamma_0 = \sum_{s=i,n} n_s \int_{-\infty}^{0} dv_\parallel \left|v_\parallel\right| g_s(z=0, v_\parallel, t) \tag{79}$$

and

$$\Gamma_{L_z} = \sum_{s=i,n} n_s \int_{0}^{\infty} dv_\parallel \left|v_\parallel\right| g_s(z=L_z, v_\parallel, t). \tag{80}$$

*4.3. Density and parallel flow evolution*

We consider the wall boundary conditions in terms of the normalised distribution function $g_s$ given in Eq. (12) and the peculiar velocity $w_\parallel = v_\parallel - u_s$. The boundary conditions on the ions and neutrals are

$$g_i(z=0, w_\parallel > -u_i, t) = 0 = g_i(z=L_z, w_\parallel < -u_i, t) \tag{81}$$

and

$$\begin{aligned} g_n(z=0, w_\parallel > -u_n, t) &= \frac{\Gamma_0}{n_n} f_{Kw}(w_\parallel + u_n), \\ g_n(z=L_z, w_\parallel < -u_n, t) &= \frac{\Gamma_{L_z}}{n_n} f_{Kw}(w_\parallel + u_n), \end{aligned} \tag{82}$$

with the Knudsen cosine distribution given by (59) and the fluxes toward the wall at the domain boundaries

$$\Gamma_0 = \sum_{s=i,n} n_s \int_{-\infty}^{-u_s} dw_\parallel \left|w_\parallel + u_s\right| g_s(z=0, w_\parallel, t) \tag{83}$$

and

$$\Gamma_{L_z} = \sum_{s=i,n} n_s \int_{-u_n}^{\infty} dw_\parallel \left|w_\parallel + u_s\right| g_s(z=L_z, w_\parallel, t). \tag{84}$$

Note that the region in $w_\parallel$ over which the boundary conditions are imposed depends on $u_s$, which evolves in time. This makes imposition of wall boundary conditions in a code difficult, if not infeasible.

### *4.4. Density and parallel pressure evolution*

In this subsection we express the wall boundary conditions in terms of the normalised distribution function $\hat{g}_s$ given by Eq. (26) and the normalised velocity $\hat{v}_\parallel = v_\parallel / v_{\mathrm{th},s}$. The boundary conditions on the ions and neutrals are

$$\hat{g}_i(z=0,\hat{v}_\parallel>0,t) = 0 = \hat{g}_i(z=L_z,\hat{v}_\parallel<0,t) \tag{85}$$

and

$$\begin{aligned} \hat{g}_n(z=0,\hat{v}_\parallel>0,t) &= \frac{v_{\mathrm{th},n}}{n_n}\Gamma_0 f_{Kw}(\hat{v}_\parallel v_{\mathrm{th},n}), \\ \hat{g}_n(z=L_z,\hat{v}_\parallel<0,t) &= \frac{v_{\mathrm{th},n}}{n_n}\Gamma_{L_z} f_{Kw}(\hat{v}_\parallel v_{\mathrm{th},n}), \end{aligned} \tag{86}$$

with the Knudsen cosine distribution given by (59) and the fluxes toward the wall at the domain boundaries

$$\Gamma_0 = \sum_{s=i,n} n_s v_{\mathrm{th},s} \int_{-\infty}^{0} d\hat{v}_\parallel \left|\hat{v}_\parallel\right| \hat{g}_s(z=0,\hat{v}_\parallel,t) \tag{87}$$

and

$$\Gamma_{L_z} = \sum_{s=i,n} n_s v_{\mathrm{th},s} \int_{0}^{\infty} d\hat{v}_\parallel \left|\hat{v}_\parallel\right| \hat{g}_s(z=L_z,\hat{v}_\parallel,t). \tag{88}$$

### *4.5. Density, parallel flow and parallel pressure evolution*

In this subsection we express the wall boundary conditions in terms of the normalised distribution function $\hat{g}_s$ given by Eq. (44) and the normalised velocity $\hat{w}_\parallel = (v_\parallel - u_s)/v_{\mathrm{th},s}$. The boundary conditions on the ions and neutrals are

$$\hat{g}_i(z=0,\hat{w}_\parallel>-u_s/v_{\mathrm{th},s},t) = 0 = \hat{g}_i(z=L_z,\hat{w}_\parallel<-u_s/v_{\mathrm{th},s},t) \tag{89}$$

and

$$\begin{aligned} \hat{g}_n(z=0,\hat{w}_\parallel>-u_s/v_{\mathrm{th},s},t) &= \frac{v_{\mathrm{th},n}}{n_n}\Gamma_0 f_{Kw}(\hat{w}_\parallel v_{\mathrm{th},n}+u_n), \\ \hat{g}_n(z=L_z,\hat{w}_\parallel<-u_s/v_{\mathrm{th},s},t) &= \frac{v_{\mathrm{th},n}}{n_n}\Gamma_{L_z} f_{Kw}(\hat{w}_\parallel v_{\mathrm{th},n}+u_n), \end{aligned} \tag{90}$$

with the Knudsen cosine distribution given by (59) and the fluxes toward the wall at the domain boundaries

$$\Gamma_0 = \sum_{s=i,n} n_s \int_{-\infty}^{-u_s/v_{\mathrm{th},s}} d\hat{w}_\parallel \left|\hat{w}_\parallel v_{\mathrm{th},s}+u_s\right| \hat{g}_s(z=0,\hat{w}_\parallel,t) \tag{91}$$

and

$$\Gamma_{L_z} = \sum_{s=i,n} n_s \int_{-u_s/v_{\mathrm{th},s}}^{\infty} d\hat{w}_\parallel \left|\hat{w}_\parallel v_{\mathrm{th},s}+u_s\right| \hat{g}_s(z=L_z,\hat{w}_\parallel,t). \tag{92}$$

Note that the region in $\hat{w}_\parallel$ over which the boundary conditions are imposed depends on $u_s$ and $v_{\mathrm{th},s}$, which evolve in time. This makes imposition of wall boundary conditions in a code difficult, if not infeasible.

| normalised variable | definition |
|---|---|
| $\tilde{t}$ | $t(c_s/L_z)$ |
| $\tilde{z}$ | $z/L_z$ |
| $\tilde{v}_\parallel$ | $v_\parallel/c_s$ |
| $\tilde{w}_\parallel$ | $w_\parallel/c_s$ |
| $\hat{v}_\parallel$ | $v_\parallel/v_{\mathrm{th},s}$ |
| $\tilde{n}_s$ | $n_s/N_e$ |
| $\tilde{u}_s$ | $u_s/c_s$ |
| $\tilde{p}_{\parallel,s}$ | $p_{\parallel,s}/(m_s N_e c_s^2)$ |
| $\tilde{T}_{\parallel,s}$ | $T_{\parallel,s}/(m_s c_s^2)$ |
| $\tilde{v}_{\mathrm{th},s}$ | $v_{\mathrm{th},s}/c_s$ |
| $\tilde{q}_{\parallel,s}$ | $q_{\parallel,s}/(m_s N_e c_s^3)$ |
| $\tilde{\phi}$ | $e\phi/T_e$ |
| $\tilde{R}_{\mathrm{in}}$ | $R_{\mathrm{in}}(N_e L_z/c_s)$ |
| $\tilde{R}_{\mathrm{ion}}$ | $R_{\mathrm{ion}}(N_e L_z/c_s)$ |
| $\tilde{f}_s$ | $f_s(\sqrt{\pi}c_s/N_e)$ |

**Table 1.** Definitions for normalised quantities used in the paper. The sound speed $c_s = \sqrt{2T_e/m_i}$, and $N_e$ and $T_e$ are the space- and time-independent density and temperature, respectively, appearing in the Boltzmann response (4).

## 5. Normalisation

In this section we define the normalisations used when solving the model equations from Secs. 2 and 3 numerically. A set of normalisations that apply regardless of the choices made for the modified distribution function and the parallel velocity coordinate is given in Table 1. Model-specific normalisations and the normalised equations for each specific moment kinetic model are provided in the following sub-sections.

Using the definitions given in Table 1 in the standard drift kinetic system of equations (1)-(4) gives

$$\frac{\partial \tilde{f}_i}{\partial \tilde{t}} + \tilde{v}_\parallel \frac{\partial \tilde{f}_i}{\partial \tilde{z}} - \frac{1}{2}\frac{\partial \tilde{\phi}}{\partial \tilde{z}}\frac{\partial \tilde{f}_i}{\partial \tilde{v}_\parallel} = -\tilde{R}_{\mathrm{in}}\left(\tilde{n}_n \tilde{f}_i - \tilde{n}_i \tilde{f}_n\right) + \tilde{R}_{\mathrm{ion}}\tilde{n}_i \tilde{f}_n, \tag{93}$$

$$\frac{\partial \tilde{f}_n}{\partial \tilde{t}} + \tilde{v}_\parallel \frac{\partial \tilde{f}_n}{\partial \tilde{z}} = -\tilde{R}_{\mathrm{in}}\left(\tilde{n}_i \tilde{f}_n - \tilde{n}_n \tilde{f}_i\right) - \tilde{R}_{\mathrm{ion}}\tilde{n}_i \tilde{f}_n, \tag{94}$$

$$e^{\tilde{\phi}} = \tilde{n}_i = \frac{1}{\sqrt{\pi}}\int_{-\infty}^{\infty} d\tilde{v}_\parallel \tilde{f}_i, \tag{95}$$

and

$$\tilde{n}_n = \frac{1}{\sqrt{\pi}}\int_{-\infty}^{\infty} d\tilde{v}_\parallel \tilde{f}_n. \tag{96}$$

The normalised forms for the wall boundary conditions given by Eqs. (57)-(61) are

$$\tilde{f}_i\left(\tilde{z}=0, \tilde{v}_\parallel > 0, \tilde{t}\right) = 0 = \tilde{f}_i\left(\tilde{z}=1, \tilde{v}_\parallel < 0, \tilde{t}\right) \tag{97}$$

and

$$\tilde{f}_n\left(\tilde{z}=0,\tilde{v}_\parallel>0,\tilde{t}\right)=\tilde{\Gamma}_0(\tilde{t})\tilde{f}_{Kw}(\tilde{v}_\parallel),\quad \tilde{f}_n\left(\tilde{z}=1,\tilde{v}_\parallel<0,\tilde{t}\right)=\tilde{\Gamma}_{L_z}(\tilde{t})\tilde{f}_{Kw}(\tilde{v}_\parallel), \tag{98}$$

where

$$\tilde{f}_{Kw}(\tilde{v}_\parallel)=c_s^2 f_{Kw}(\tilde{v}_\parallel c_s)=\frac{3\sqrt{\pi}}{\tilde{T}_w^{3/2}}\left|\tilde{v}_\parallel\right|\operatorname{erfc}\left(\frac{\left|\tilde{v}_\parallel\right|}{\sqrt{\tilde{T}_w}}\right), \tag{99}$$

$$\tilde{\Gamma}_0(\tilde{t})=\sum_{s=i,n}\int_{-\infty}^{0}d\tilde{v}_\parallel\left|\tilde{v}_\parallel\right|\tilde{f}_s(\tilde{z}=0,\tilde{v}_\parallel,\tilde{t}), \tag{100}$$

and

$$\tilde{\Gamma}_{L_z}(\tilde{t})=\sum_{s=i,n}\int_{0}^{\infty}d\tilde{v}_\parallel\left|\tilde{v}_\parallel\right|\tilde{f}_s(\tilde{z}=1,\tilde{v}_\parallel,\tilde{t}), \tag{101}$$

with $\tilde{T}_w \doteq T_w/T_e$.

### *5.1. Density evolution*

We define the normalised distribution function

$$\tilde{g}_s \doteq g_s c_s\sqrt{\pi}. \tag{102}$$

In terms of this normalised distribution function and the normalised quantities defined in Table 1, Eqs. (9)-(11) become

$$\frac{\partial\tilde{n}_s}{\partial\tilde{t}}+\frac{\partial\tilde{n}_s\tilde{u}_s}{\partial\tilde{z}}=\pm\tilde{R}_{\text{ion}}\tilde{n}_i\tilde{n}_n \tag{103}$$

$$\frac{\partial\tilde{g}_i}{\partial\tilde{t}}+\frac{\tilde{v}_\parallel}{\tilde{n}_i}\frac{\partial\tilde{f}_i}{\partial\tilde{z}}-\frac{1}{2}\frac{\partial\tilde{\phi}}{\partial\tilde{z}}\frac{\partial\tilde{g}_i}{\partial\tilde{v}_\parallel}=\frac{\tilde{g}_i}{\tilde{n}_i}\frac{\partial\tilde{n}_i\tilde{u}_\text{i}}{\partial\tilde{z}}+\left(\tilde{R}_{\text{in}}+\tilde{R}_{\text{ion}}\right)\tilde{n}_n\left(\tilde{g}_n-\tilde{g}_\text{i}\right), \tag{104}$$

and

$$\frac{\partial\tilde{g}_n}{\partial\tilde{t}}+\frac{\tilde{v}_\parallel}{\tilde{n}_n}\frac{\partial\tilde{f}_n}{\partial\tilde{z}}=\frac{\tilde{g}_n}{\tilde{n}_n}\frac{\partial\tilde{n}_n\tilde{u}_n}{\partial\tilde{z}}-\tilde{R}_{\text{in}}\tilde{n}_i\left(\tilde{g}_n-\tilde{g}_i\right). \tag{105}$$

The normalised forms for the wall boundary conditions (77)-(80) are

$$\tilde{g}_i(\tilde{z}=0,\tilde{v}_\parallel>0,\tilde{t})=0=\tilde{g}_i(\tilde{z}=1,\tilde{v}_\parallel<0,\tilde{t}), \tag{106}$$

$$\begin{aligned}\tilde{g}_n(\tilde{z}=0,\tilde{v}_\parallel>0,\tilde{t})&=\frac{\tilde{\Gamma}_0}{\tilde{n}_n}\tilde{f}_{Kw}(\tilde{v}_\parallel),\\ \tilde{g}_n(\tilde{z}=1,\tilde{v}_\parallel<0,\tilde{t})&=\frac{\tilde{\Gamma}_{L_z}}{\tilde{n}_n}\tilde{f}_{Kw}(\tilde{v}_\parallel),\end{aligned} \tag{107}$$

with the normalised Knudsen cosine distribution given by Eq. (99) and the normalised fluxes toward the walls

$$\tilde{\Gamma}_0=\sum_{s=i,n}\tilde{n}_s\int_{-\infty}^{0}d\tilde{v}_\parallel\left|\tilde{v}_\parallel\right|\tilde{g}_s(\tilde{z}=0,\tilde{v}_\parallel,\tilde{t}) \tag{108}$$

and

$$\tilde{\Gamma}_{L_z}=\sum_{s=i,n}\tilde{n}_s\int_{0}^{\infty}d\tilde{v}_\parallel\left|\tilde{v}_\parallel\right|\tilde{g}_s(\tilde{z}=1,\tilde{v}_\parallel,\tilde{t}). \tag{109}$$

*5.2. Density and parallel flow evolution*

We use the normalised distribution function (102) and define

$$\tilde{w}_\parallel \doteq \frac{w_\parallel}{c_s}. \tag{110}$$

Using these normalised quantities and the definitions given in Table 1, Eqs. (9), (21), (24) and (25) become

$$\frac{\partial \tilde{n}_s}{\partial \tilde{t}} + \frac{\partial \tilde{n}_s \tilde{u}_s}{\partial \tilde{z}} = \pm \tilde{R}_{\rm ion} \tilde{n}_i \tilde{n}_n \tag{111}$$

$$\frac{\partial \left(\tilde{n}_s \tilde{u}_s\right)}{\partial \tilde{t}} = -\frac{\partial \left(\tilde{p}_{\parallel,s} + \tilde{n}_s \tilde{u}_s^2\right)}{\partial \tilde{z}} - \delta_{s,i} \frac{\tilde{n}_s}{2} \frac{\partial \tilde{\phi}}{\partial \tilde{z}} + \tilde{R}_{\rm in} \tilde{n}_s \tilde{n}_{s'} \left(\tilde{u}_{s'} - \tilde{u}_s\right) \pm \tilde{R}_{\rm ion} \tilde{n}_s \tilde{n}_{s'} \tilde{u}_n \tag{112}$$

and

$$\frac{\partial \tilde{g}_s}{\partial \tilde{t}} + \frac{\left(\tilde{w}_\parallel + \tilde{u}_s\right)}{\tilde{n}_s} \frac{\partial \tilde{f}_s}{\partial \tilde{z}} + \dot{\tilde{w}}_{\parallel,s} \frac{\partial \tilde{g}_s}{\partial \tilde{w}_\parallel} = \tilde{g}_s \frac{\partial \tilde{n}_s \tilde{u}_s}{\partial \tilde{z}} + \left(\tilde{R}_{\rm in} + \delta_{s,i} \tilde{R}_{\rm ion}\right) \tilde{n}_{s'} \left(\tilde{g}_{s'} - \tilde{g}_s\right), \tag{113}$$

where the top (bottom) sign in Eq. (112) corresponds to ions (neutrals), and

$$\dot{\tilde{w}}_{\parallel,s} \doteq \dot{w}_{\parallel,s} \frac{L_z}{c_s^2} = \frac{1}{\tilde{n}_s} \frac{\partial \tilde{p}_{\parallel,s}}{\partial \tilde{z}} - \left(\tilde{R}_{\rm in} + \delta_{s,i} \tilde{R}_{\rm ion}\right) \tilde{n}_{s'} \left(\tilde{u}_{s'} - \tilde{u}_s\right) - \tilde{w}_\parallel \frac{\partial \tilde{u}_s}{\partial \tilde{z}}. \tag{114}$$

The normalised forms for the wall boundary conditions (81)-(84) are

$$\tilde{g}_i(\tilde{z} = 0, \tilde{w}_\parallel > -\tilde{u}_i, \tilde{t}) = 0 = \tilde{g}_i(\tilde{z} = 1, \tilde{w}_\parallel < -\tilde{u}_i, \tilde{t}), \tag{115}$$

and

$$\begin{aligned} \tilde{g}_n(\tilde{z} = 0, \tilde{w}_\parallel > -\tilde{u}_n, \tilde{t}) &= \frac{\tilde{\Gamma}_0}{\tilde{n}_n} \tilde{f}_{Kw}(\tilde{w}_\parallel + \tilde{u}_n), \\ \tilde{g}_n(\tilde{z} = 1, \tilde{w}_\parallel < -\tilde{u}_n, \tilde{t}) &= \frac{\tilde{\Gamma}_{L_z}}{\tilde{n}_n} \tilde{f}_{Kw}(\tilde{w}_\parallel + \tilde{u}_n), \end{aligned} \tag{116}$$

with the normalised Knudsen cosine distribution $\tilde{f}_{Kw}$ given by Eq. (99) and the normalised fluxes toward the walls

$$\tilde{\Gamma}_0 = \sum_{s=i,n} \tilde{n}_s \int_{-\infty}^{-\tilde{u}_s} d\tilde{w}_\parallel \left|\tilde{w}_\parallel + \tilde{u}_s\right| \tilde{g}_s(\tilde{z} = 0, \tilde{w}_\parallel, \tilde{t}) \tag{117}$$

and

$$\tilde{\Gamma}_{L_z} = \sum_{s=i,n} \tilde{n}_s \int_{-\tilde{u}_s}^{\infty} d\tilde{w}_\parallel \left|\tilde{w}_\parallel + \tilde{u}_s\right| \tilde{g}_s(\tilde{z} = 1, \tilde{w}_\parallel, \tilde{t}). \tag{118}$$

### *5.3. Density and parallel pressure evolution*

We use the already-normalised distribution function $\hat{g}_s$ defined in Eq. (26). In terms of this normalised distribution function and the normalised quantities defined in Table 1, Eqs. (9), (39), (42) and (43) become

$$\frac{\partial \tilde{n}_s}{\partial \tilde{t}} + \frac{\partial \tilde{n}_s \tilde{u}_s}{\partial \tilde{z}} = \pm \tilde{R}_{\text{ion}} \tilde{n}_i \tilde{n}_n, \tag{119}$$

$$\frac{\partial \tilde{p}_{\parallel,s}}{\partial \tilde{t}} + \tilde{u}_s \frac{\partial \tilde{p}_{\parallel,s}}{\partial \tilde{z}} = -\frac{\partial \tilde{q}_{\parallel,s}}{\partial \tilde{z}} - 3\tilde{p}_{\parallel,s} \frac{\partial \tilde{u}_s}{\partial \tilde{z}} - \tilde{R}_{\text{ss'}} \left( \tilde{n}_{s'} \tilde{p}_{\parallel,s} - \tilde{n}_s \tilde{p}_{\parallel,s'} \right) \pm \tilde{R}_{\text{ion}} \tilde{n}_i \tilde{p}_{\parallel,n}, \tag{120}$$

$$\begin{aligned} \frac{\partial \hat{g}_s}{\partial \tilde{t}} + \frac{\tilde{v}_{\text{th},s}^2}{\tilde{n}_s} \hat{v}_\parallel \frac{\partial \tilde{f}_s}{\partial \tilde{z}} + \dot{\tilde{\hat{v}}}_{\parallel,s} \frac{\partial \hat{g}_s}{\partial \hat{v}_\parallel} &= \hat{g}_s \tilde{u}_s \left( \frac{\partial \ln \tilde{n}_s}{\partial \tilde{z}} - \frac{\partial \ln \tilde{v}_{\text{th},s}}{\partial \tilde{z}} \right) - \frac{\hat{g}_s}{2\tilde{p}_{\parallel,s}} \frac{\partial \tilde{q}_{\parallel,s}}{\partial \tilde{z}} \\ &- \left( \tilde{R}_{\text{ss'}} + \delta_{s,i} \tilde{R}_{\text{ion}} \right) \tilde{n}_{s'} \left( \hat{g}_s - \hat{g}_{s'} \frac{\tilde{v}_{\text{th},s}}{\tilde{v}_{\text{th},s'}} \right) + \hat{g}_s \left( \frac{\tilde{n}_{s'}}{2} \left( \tilde{R}_{\text{ss'}} + \delta_{s,i} \tilde{R}_{\text{ion}} \right) \left( \frac{\tilde{T}_{\parallel,s'}}{\tilde{T}_{\parallel,s}} - 1 \right) \right), \end{aligned} \tag{121}$$

and

$$\begin{aligned} \dot{\tilde{\hat{v}}}_{\parallel,s} = &- \left( \frac{\delta_{s,i}}{2\tilde{v}_{\text{th},s}} \frac{\partial \tilde{\phi}}{\partial \tilde{z}} + \tilde{v}_{\text{th},s} \hat{v}_\parallel^2 \frac{\partial \ln \tilde{v}_{\text{th},s}}{\partial \tilde{z}} \right) \\ &+ \hat{v}_\parallel \left( \frac{\tilde{n}_{s'}}{2} \left( \tilde{R}_{\text{ss'}} + \delta_{s,i} \tilde{R}_{\text{ion}} \right) \left( 1 - \frac{\tilde{T}_{\parallel,s'}}{\tilde{T}_{\parallel,s}} \right) + \frac{1}{\tilde{v}_{\text{th},s}} \frac{\partial \tilde{u}_s \tilde{v}_{\text{th},s}}{\partial \tilde{z}} + \frac{1}{2\tilde{p}_{\parallel,s}} \frac{\partial \tilde{q}_{\parallel,s}}{\partial \tilde{z}} \right). \end{aligned} \tag{122}$$

The normalised forms for the wall boundary conditions (85)-(88) are

$$\hat{g}_i(\tilde{z} = 0, \hat{v}_\parallel > 0, \tilde{t}) = 0 = \hat{g}_i(\tilde{z} = 1, \hat{v}_\parallel < 0, \tilde{t}), \tag{123}$$

and

$$\begin{aligned} \hat{g}_n(\tilde{z} = 0, \hat{v}_\parallel > 0, \tilde{t}) &= \frac{\tilde{v}_{\text{th},n}}{\tilde{n}_n} \tilde{\Gamma}_0 \tilde{f}_{Kw}(\hat{v}_\parallel \tilde{v}_{\text{th},n}), \\ \hat{g}_n(\tilde{z} = 1, \hat{v}_\parallel < 0, \tilde{t}) &= \frac{\tilde{v}_{\text{th},n}}{\tilde{n}_n} \tilde{\Gamma}_{L_z} \tilde{f}_{Kw}(\hat{v}_\parallel \tilde{v}_{\text{th},n}), \end{aligned} \tag{124}$$

with the normalised Knudsen cosine distribution $\tilde{f}_{Kw}$ given by Eq. (99) and the normalised fluxes toward the walls

$$\tilde{\Gamma}_0 = \sum_{s=i,n} \tilde{n}_s \tilde{v}_{\text{th},s} \int_{-\infty}^{0} d\hat{v}_\parallel \left| \hat{v}_\parallel \tilde{v}_{\text{th},s} \right| \hat{g}_s(\tilde{z} = 0, \hat{v}_\parallel, \tilde{t}) \tag{125}$$

and

$$\tilde{\Gamma}_{L_z} = \sum_{s=i,n} \tilde{n}_s \tilde{v}_{\text{th},s} \int_{0}^{\infty} d\hat{v}_\parallel \left| \hat{v}_\parallel \tilde{v}_{\text{th},s} \right| \hat{g}_s(\tilde{z} = 1, \hat{v}_\parallel \tilde{t}). \tag{126}$$

### *5.4. Density, parallel flow and parallel pressure evolution*

We use the normalised distribution function (44) and the normalised peculiar velocity $\hat{w}_\parallel = w_\parallel/v_{\mathrm{th},s}$. In terms of these normalised quantities and those defined in Table 1, Eqs. (9), (21), (39), (47) and (48) become Eqs. (103), (112), (120),

$$\begin{aligned}\frac{\partial \hat{g}_s}{\partial \tilde{t}} + \frac{\tilde{v}_{\mathrm{th},s}}{\tilde{n}_s}\left(\tilde{v}_{\mathrm{th},s}\hat{w}_\parallel + \tilde{u}_s\right)\frac{\partial \tilde{f}_s}{\partial \tilde{z}} + \dot{\hat{w}}_{\parallel,s}\frac{\partial \hat{g}_s}{\partial \hat{w}_\parallel} = \hat{g}_s\tilde{u}_s\left(\frac{\partial \ln \tilde{n}_s}{\partial \tilde{z}} - \frac{\partial \ln \tilde{v}_{\mathrm{th},s}}{\partial \tilde{z}}\right) - \frac{\hat{g}_s}{2\tilde{p}_{\parallel,s}}\frac{\partial \tilde{q}_{\parallel,s}}{\partial \tilde{z}} \\ - \left(\tilde{R}_{\mathrm{ss'}} + \delta_{s,i}R_{\mathrm{ion}}\right)\tilde{n}_{s'}\left(\hat{g}_s - \frac{\tilde{v}_{\mathrm{th},s}}{\tilde{v}_{\mathrm{th},s'}}\hat{g}_{s'}\right) + \hat{g}_s\left(\frac{\tilde{n}_{s'}}{2}\left(\tilde{R}_{\mathrm{ss'}} + \delta_{s,i}\tilde{R}_{\mathrm{ion}}\right)\left(\frac{\tilde{T}_{\parallel,s'}}{\tilde{T}_{\parallel,s}} - 1\right)\right),\end{aligned} \tag{127}$$

and

$$\begin{aligned}\dot{\hat{w}}_{\parallel,s} = -w_\parallel^2\frac{\partial \tilde{v}_{\mathrm{th},s}}{\partial \tilde{z}} + \frac{1}{\tilde{v}_{\mathrm{th},s}}\left(\frac{1}{\tilde{n}_s}\frac{\partial \tilde{p}_{\parallel,s}}{\partial \tilde{z}} - \left(\tilde{R}_{\mathrm{ss'}} + \delta_{si}\tilde{R}_{\mathrm{ion}}\right)\tilde{n}_{s'}\left(\tilde{u}_{s'} - \tilde{u}_s\right)\right) \\ + \frac{w_\parallel}{2\tilde{p}_{\parallel,s}}\left(\frac{\partial \tilde{q}_{\parallel,s}}{\partial z} + \left(\tilde{R}_{\mathrm{ss'}} + \delta_{si}R_{\mathrm{ion}}\right)\left(\tilde{n}_{s'}\tilde{p}_{\parallel,s} - \tilde{n}_s\tilde{p}_{\parallel,s'}\right)\right),\end{aligned} \tag{128}$$

The normalised forms for the wall boundary conditions (89)-(92) are

$$\hat{g}_i(\tilde{z}=0, \hat{w}_\parallel > -\tilde{u}_s/\tilde{v}_{\mathrm{th},s}, \tilde{t}) = 0 = \hat{g}_i(\tilde{z}=1, \hat{w}_\parallel < -\tilde{u}_s/\tilde{v}_{\mathrm{th},s}, \tilde{t}) \tag{129}$$

and

$$\begin{aligned}\hat{g}_n(\tilde{z}=0, \hat{w}_\parallel > -\tilde{u}_s/\tilde{v}_{\mathrm{th},s}, t) = \frac{\tilde{v}_{\mathrm{th},n}}{\tilde{n}_n}\tilde{\Gamma}_0(\tilde{t})\tilde{f}_{Kw}(\hat{w}_\parallel\tilde{v}_{\mathrm{th},n} + \tilde{u}_n), \\ \hat{g}_n(\tilde{z}=1, \hat{w}_\parallel < -\tilde{u}_s/\tilde{v}_{\mathrm{th},s}, t) = \frac{\tilde{v}_{\mathrm{th},n}}{\tilde{n}_n}\tilde{\Gamma}_{L_z}(\tilde{t})\tilde{f}_{Kw}(\hat{w}_\parallel\tilde{v}_{\mathrm{th},n} + \tilde{u}_n),\end{aligned} \tag{130}$$

with the normalised Knudsen cosine distribution $\tilde{f}_{Kw}$ given by Eq. (99) and the normalised fluxes toward the walls

$$\tilde{\Gamma}_0(\tilde{t}) = \frac{\Gamma_0}{N_e c_s} = \sum_{s=i,n}\tilde{n}_s\int_{-\infty}^{-\tilde{u}_s/\tilde{v}_{\mathrm{th},s}} d\hat{w}_\parallel \left|\hat{w}_\parallel\tilde{v}_{\mathrm{th},s} + \tilde{u}_s\right| \hat{g}_s(\tilde{z}=0, \hat{w}_\parallel, \tilde{t}), \tag{131}$$

and

$$\tilde{\Gamma}_{L_z}(\tilde{t}) = \frac{\Gamma_{L_z}}{N_e c_s} = \sum_{s=i,n}\tilde{n}_s\int_{-\tilde{u}_s/\tilde{v}_{\mathrm{th},s}}^{\infty} d\hat{w}_\parallel \left|\hat{w}_\parallel\tilde{v}_{\mathrm{th},s} + \tilde{u}_s\right| \hat{g}_s(\tilde{z}=1, \hat{w}_\parallel, \tilde{t}). \tag{132}$$

## 6. Numerical implementation

The algorithms described in this Section have been implemented in the code, written in the Julia programming language, currently available on GitHub at `https://github.com/mabarnes/moment_kinetics`.

### *6.1. Time advance*

We evolve the normalised systems of equations described in Sec. 5 using a time-marching scheme (as opposed to an eigensolver) due to its efficiency and due to the nonlinear nature of the system of partial differential equations under consideration. In particular, we employ a member of the family of Strong Stability Preserving (SSP) Runge-Kutta (RK) schemes; see, e.g., [8, 9, 10]. Current SSPRK options implemented in the code are SSPRK1 (forward Euler), SSPRK2 (Heun's method) SSPRK3 (Shu-Osher method) and four-stage SSPRK3. The user can also specify the use of 'flip-flop' Lie operator splitting. Operator splitting limits the time advance scheme to second order accuracy in step size, but could be useful for separately treating different pieces of physics. Here we describe the current default option, which is the four-stage SSPRK3 method without operator splitting.

For convenience of notation, we express the normalised drift kinetic and moment kinetic equations for the ions and neutrals in the vector form

$$\frac{\partial \mathbf{f}}{\partial t} = G[\mathbf{f}], \tag{133}$$

with $\mathbf{f}$ the solution vector containing the evolved quantities; e.g., $\mathbf{f} = (\hat{g}_i, \hat{g}_n, \tilde{n}_i, \tilde{n}_n, \tilde{u}_i, \tilde{u}_n, \tilde{p}_{\parallel,i}, \tilde{p}_{\parallel,n})^T$ if all of the low-order moments are evolved separately from the pdf. The operator $G$ accounts for all effects that lead to the evolution of $\mathbf{f}$, e.g., parallel streaming, parallel acceleration, charge exchange and ionisation collisions, as well as all terms in the continuity, force balance and energy equations if they are separately evolved. The four-stage SSPRK3 method for advancing this system of equations is 3rd order accurate in time step size $\Delta t$, with a Courant number of two. It is given by

$$\begin{aligned}
\mathbf{f}^{(1)} &= \frac{1}{2}\mathbf{f}^n + \frac{1}{2}\left(\mathbf{f}^n + \Delta t G\left[\mathbf{f}^n\right]\right), \\
\mathbf{f}^{(2)} &= \frac{1}{2}\mathbf{f}^{(1)} + \frac{1}{2}\left(\mathbf{f}^{(1)} + \Delta t G\left[\mathbf{f}^{(1)}\right]\right), \\
\mathbf{f}^{(3)} &= \frac{2}{3}\mathbf{f}^n + \frac{1}{6}\mathbf{f}^{(2)} + \frac{1}{6}\left(\mathbf{f}^{(2)} + \Delta t G\left[\mathbf{f}^{(2)}\right]\right), \\
\mathbf{f}^{n+1} &= \frac{1}{2}\mathbf{f}^{(3)} + \frac{1}{2}\left(\mathbf{f}^{(3)} + \Delta t G\left[\mathbf{f}^{(3)}\right]\right),
\end{aligned} \tag{134}$$

where the superscript $n$ denotes the time level.

We have tested our implementation of SSP RK2 and 4-stage SSP RK3 by calculating the rms error in the distribution function after it is advected in one dimension with constant advection speed for ten transits of the $\tilde{z}$ domain:

$$\epsilon_{\mathrm{rms}} \doteq \sqrt{\frac{1}{N_z}\sum_{j=1}^{N_z} \left|f_i(z_j, t=10) - f_i(z_j, t=0)\right|^2}. \tag{135}$$

Example data are given for a case in which the standard drift kinetic equations from Sec. 5 are solved with $\tilde{v} = 1$. The results when paired with a finite difference discretisation (third order upwind) are given in Fig. 1. For Chebyshev pseudospectral discretisation on a single element with 4-stage SSPRK3, see Fig. 2.

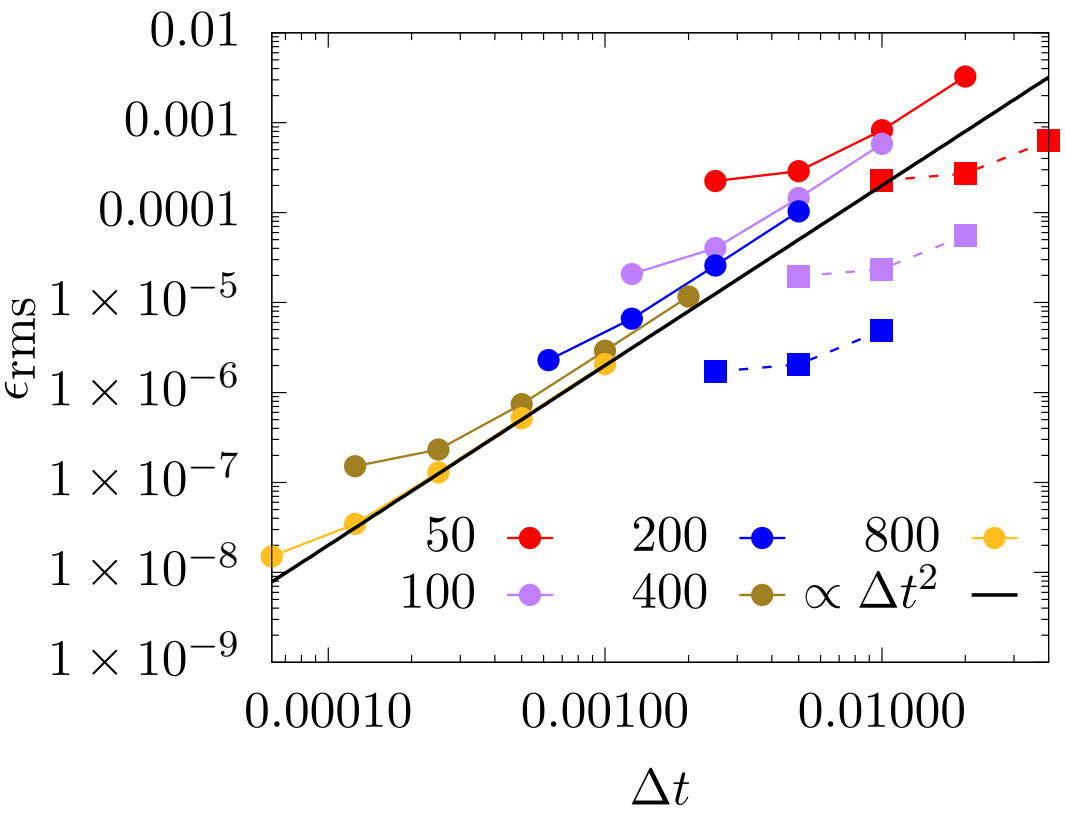


**Figure 1.** RMS error as a function of time step size $\Delta t$ and varying values for $N_z$ for both SSP RK2 (solid lines and circles) and for 4-stage SSP RK3 (dashed lines and squares) with a third order, upwinded finite difference discretisation. Due to the CFL restriction that ties temporal resolution to spatial resolution, the range in $\Delta t$ over which time domain errors dominate is limited for RK2 and is effectively non-existent for RK3.

### *6.2. Spatial discretisation*

There are two discretisation schemes implemented in the code: finite differences and Chebyshev (pseudo)spectral elements. The user can choose at run-time which scheme to use for each of the $z$ and $v_\parallel$ coordinates.

*6.2.1. Finite difference discretisation.* For the finite difference discretisation, the corresponding coordinate grid is uniform on the domain $[-L/2, L/2]$, with $L$ the coordinate box length. The default method employed for derivatives is 3rd order upwind differences, though 1st and 2nd order schemes are also available as options. For an overview of upwind differences and a discussion of the merits of the different upwind schemes, see, e.g. [11]. The associated integration weights used for field-line averages in $z$ and/or for the $v_\parallel$ integration required for obtaining fields/moments are obtained using the composite Simpson's rule (sometimes referred to as composite Simpson's 1/3

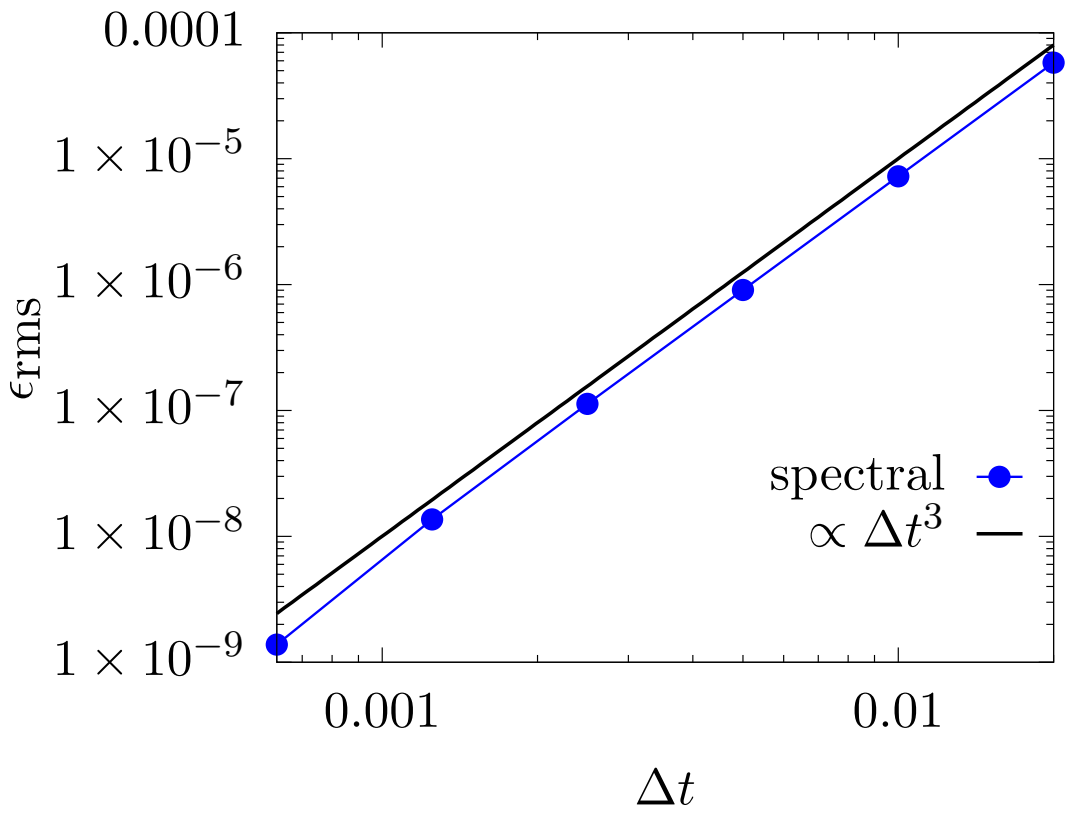


**Figure 2.** RMS error as a function of time step size $\Delta t$ for 4-stage SSP RK3 with a Chebyshev pseudospectral discretisation.

rule):

$$\int_0^L dx\ f(x) \approx \frac{h}{3} \sum_{j=1}^{(N-1)/2} \left( f(x_{2j-1}) + 4f(x_{2j}) + f(x_{2j+1}) \right), \tag{136}$$

where $N$ is the number of grid points in the coordinate $x$, and $h = L/(N-1)$ is the uniform grid spacing. The composite rule (136) is only applicable for $N$ odd, so it is supplemented at the boundary by Simpson's 3/8 rule when $N$ is even.

*6.2.2. Chebyshev spectral elements.* When using Chebyshev spectral elements, the corresponding coordinate grid is the Gauss-Chebyshev-Lobatto grid on each element. For a description of Chebyshev-Gauss quadrature, see, e.g. [12]. Inclusion of the endpoints within each element facilitates enforcement of continuity at element boundaries, and the use of Chebyshev polynomials as a basis enables the use of Fast Fourier Transforms. In our code, these transforms are done using the widely-used FFTW library [13]. The associated integration weights used for field-line averages in $z$ and/or for the $v_\parallel$ integration required for obtaining fields/moments are obtained using Clenshaw-Curtis quadrature rules [14]. Clenshaw-Curtis quadrature is convenient, as it allows for the use of endpoints in the integration domain (which is dictated by the use

of a Gauss-Chebyshev-Lobatto grid) while still exactly integrating polynomials up to degree $N-1$, with $N$ the number of points within the element.

A 1D advection test demonstrating the spectral accuracy of the Chebyshev scheme on a single element is given in Fig. 3, where the rms error is given by Eq. (135). The maximum stable time step subject to the CFL restriction is plotted as a function of the number of $z$ grid points on a single element in Fig. 4 and as a function of the number of elements $N_{\text{elem}}$ with $N_z = 9$ fixed in Fig. 5. Slight deviations from the expected scalings are likely due to the numerical dissipation that is introduced by the use of the derivative from the upwind element at the overlapping point at element boundaries and at the boundary of the periodic domain.

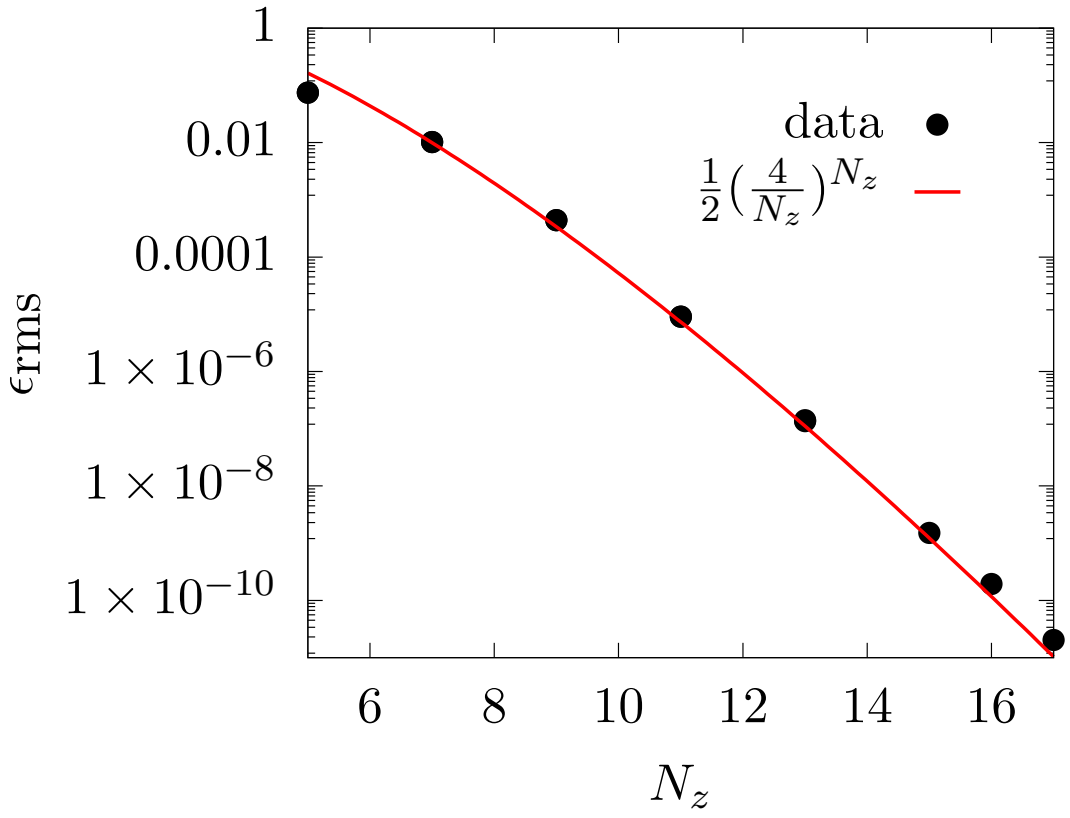


**Figure 3.** RMS error as a function of the number of grid points $N_z$. The time advance scheme used is 4-stage SSP RK3.

### *6.3. Conservation properties*

Each of the system of equations detailed in Secs. 3 and 5 have associated quantities that should be conserved: In the absence of ionisation collisions, particle number should be conserved, and certain moments of the evolved pdf should evaluate to constants; e.g., if the density, parallel flow and parallel pressure are evolved separately from the normalised pdf $\hat{g}_s$ given by Eq. (26) (as detailed in Sec. 3.4), then the system has the

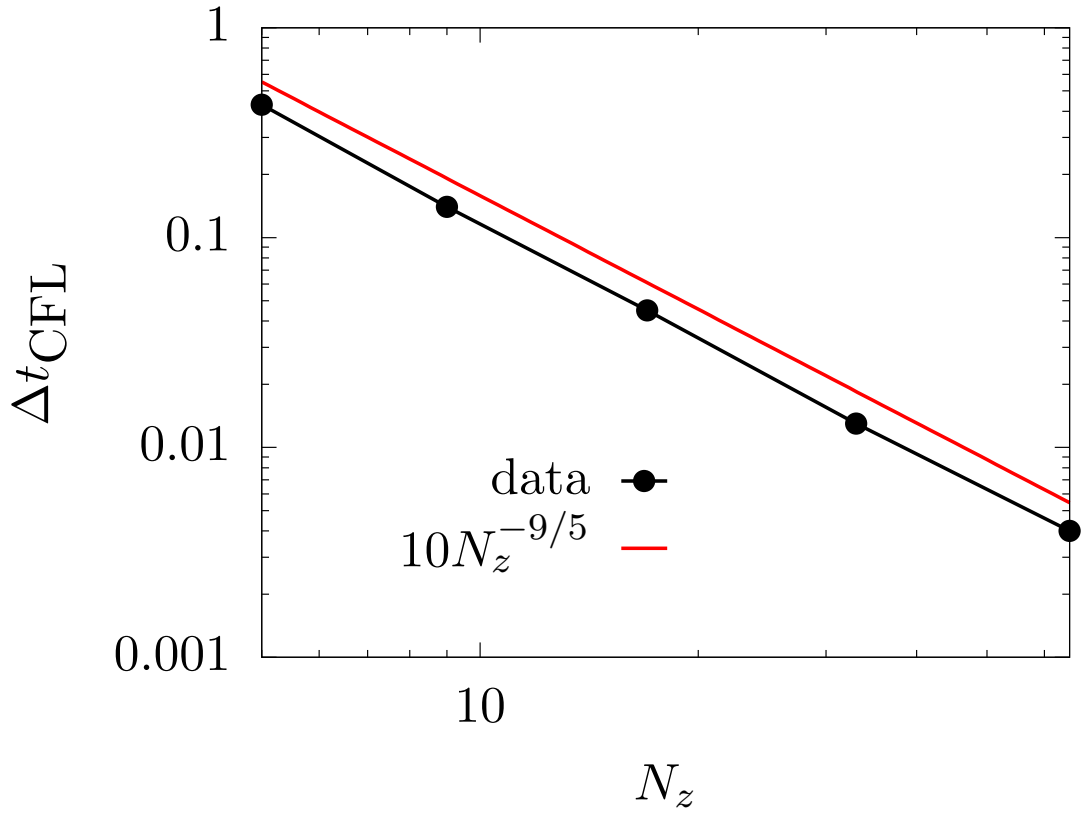


**Figure 4.** Maximum stable time step subject to the CFL restriction as a function of the number of Gauss-Chebyshev-Lobatto grid points. The max stable time step scales a bit more weakly than $1/N_z^2$, as expected.

conserved quantities $\int d\hat{w}_\parallel (1, \hat{w}_\parallel, \hat{w}_\parallel^2)\hat{g}_s = (1, 0, 1/2)$. We would like to ensure that such conservation properties are preserved by the numerical scheme.

The currently-favoured approach in the code for satisfying exactly the desired conservation properties is to correct the numerical solutions for $\tilde{n}_s$ (if it is appropriate for particle number to be conserved) and for $\tilde{g}_s$ or $\hat{g}_s$ at the end of each time step. For the particle density, one can set

$$\tilde{n}_s^{m+1} = \hat{n}_s^{m+1} + \tilde{n}_s^m \left(1 - \frac{\int d\tilde{z}\ \hat{n}_s^{m+1}}{\int d\tilde{z}\ \tilde{n}_s^m}\right), \tag{137}$$

where $\hat{n}^{m+1}$ is the updated solution (at time level $m+1$) to the continuity equation before applying any conserving correction. This guarantees that $\int d\tilde{z}\,(\tilde{n}_s^{m+1} - \tilde{n}_s^m) = 0$. The additional error in the density introduced by this correction is

$$\begin{aligned} \tilde{n}^m \left(1 - \frac{\int d\tilde{z}\ \hat{n}^{m+1}}{\int d\tilde{z}\ \tilde{n}^m}\right) &= \tilde{n}^m \left(1 - \frac{\int d\tilde{z}\ \left(\tilde{n}_{\mathrm{exact}}^{m+1} + \epsilon^m\right)}{\int d\tilde{z}\ \tilde{n}^m}\right) \\ &= \tilde{n}^m \frac{\int d\tilde{z}\ \epsilon^m}{\int d\tilde{z}\ \tilde{n}^m} = \mathcal{O}(\epsilon^m), \end{aligned} \tag{138}$$

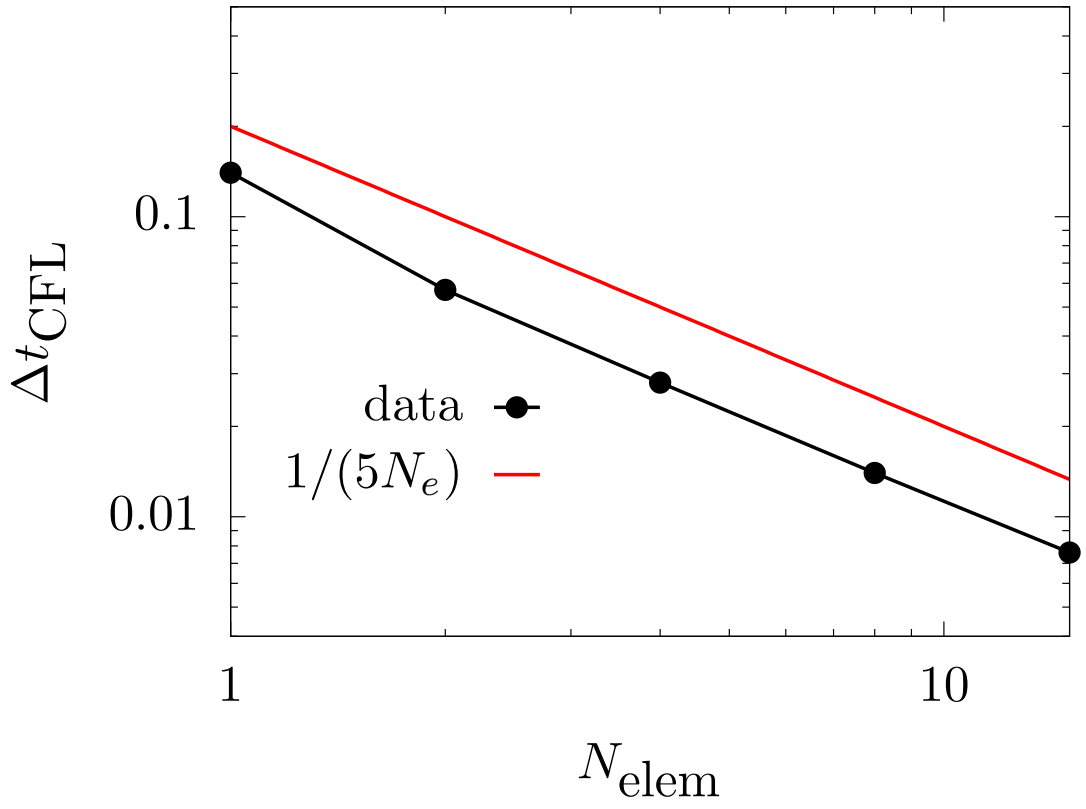


**Figure 5.** Maximum stable time step subject to the CFL restriction as a function of the number of elements with the number of grid points per element fixed at 9. The minimum grid spacing scales inversely with the number of elements, leading to a max stable time step that is inversely proportional to the number of elements $N_{\mathrm{elem}}$.

where $\epsilon^m$ is the error in $\tilde{n}^{m+1}$ due to numerical discretisation, $\tilde{n}^{m+1}_{\mathrm{exact}}$ is the solution for $\hat{n}^{m+1}$ in the limit $\epsilon^m = 0$, and species subscripts have been suppressed for convenience of notation.

A similar technique can be applied to conserve quantities such as $\int d\hat{w}_\parallel \hat{g} = 1$, $\int d\hat{w}_\parallel \hat{w}_\parallel \hat{g} = 0$ and $\int d\hat{w}_\parallel \hat{w}_\parallel^2 \hat{g} = 1/2$. As this case, where the density, parallel flow and parallel pressure are all evolved separately, encapsulates all of the issues one might encounter when enforcing exact conservation, we present our conserving treatment for it here. For such a case, we set

$$\begin{aligned}\hat{g}^{m+1} = \overline{g}^{m+1} + \hat{g}^m \left(1 - \int d\hat{w}_\parallel \overline{g}^{m+1}\right) - \frac{\partial \hat{g}^m}{\partial \hat{w}_\parallel} \frac{\int d\hat{w}_\parallel \hat{w}_\parallel \overline{g}^{m+1}}{\int d\hat{w}_\parallel \hat{w}_\parallel \left(\partial \hat{g}^m / \partial \hat{w}_\parallel\right)} \\ - \frac{\partial \hat{w}_\parallel \hat{g}^m}{\partial \hat{w}_\parallel} \frac{\int d\hat{w}_\parallel \left(\hat{w}_\parallel^2 - 1/2\right) \overline{g}^{m+1}}{\int d\hat{w}_\parallel \hat{w}_\parallel^2 \left(\partial \left(\hat{w}_\parallel \hat{g}^m\right) / \partial \hat{w}_\parallel\right)},\end{aligned} \tag{139}$$

where $\overline{g}^{m+1}$ is the updated solution to the drift kinetic equation before applying any conserving correction. The additional error in $\hat{g}$ associated with this correction is $\mathcal{O}(\delta^m)$,

where $\delta^m$ is the error in $\hat{g}^{m+1}$ associated with discretisation. The correction ensures that $\int d\hat{w}_\parallel \hat{g}^{m+1} = 1$, $\int d\hat{w}_\parallel \hat{w}_\parallel \hat{g}^{m+1} = 0$ and $\int d\hat{w}_\parallel \hat{w}_\parallel^2 \hat{g}^{m+1} = 1/2$, provided the corresponding properties are satisfied for $\hat{g}^m$.

It is thus critical to carefully choose the initial conditions in the code so that these properties are initially satisfied to machine precision. To do this we first set initial conditions on the density, parallel flow and parallel pressure profiles, and then construct the initial, normalised distribution function, $\overline{g}^0$. This initial distribution function is then corrected in a manner analogous to $\overline{g}^{m+1}$ above:

$$\hat{g}^0 = \frac{\overline{g}^0}{\int d\hat{w}_\parallel \overline{g}^0} + \left(\frac{1}{2} - \frac{\int d\hat{w}_\parallel \hat{w}_\parallel^2 \overline{g}^0}{\int d\hat{w}_\parallel \overline{g}^0}\right)\left(\frac{\hat{w}_\parallel^2 \overline{g}^0}{\int d\hat{w}_\parallel \hat{w}_\parallel^2 \overline{g}^0} - \frac{\overline{g}^0}{\int d\hat{w}_\parallel \overline{g}^0}\right) \Bigg/ \left(\int d\hat{w}_\parallel \hat{w}_\parallel^2 \left(\frac{\hat{w}_\parallel^2 \overline{g}^0}{\int d\hat{w}_\parallel \hat{w}_\parallel^2 \overline{g}^0} - \frac{\overline{g}^0}{\int d\hat{w}_\parallel \overline{g}^0}\right)\right) \tag{140}$$

This approach is simple, does not change the order of accuracy of the discretisation scheme and allows for the use of numerical dissipation to improve numerical stability properties. Furthermore, in contrast to the discretisation errors that would naturally arise when relying on a conservative differencing scheme, the error arising from this correction is easy to monitor, as it is explicitly calculable. Results showing the efficacy of these corrections are given in Sec. 7

### *6.4. Mixed velocity grids due to collisions*

When employing the parallel velocity coordinates $\tilde{w}_\parallel$ (110), $\hat{v}_\parallel$ (27) or $\hat{w}_\parallel$ (45), the ion and neutral pdfs will in general be evaluated on different $v_\parallel$ grids. This is because the mapping from each of these velocity coordinates to $v_\parallel$ depends on $\tilde{v}_{\mathrm{th},s}$ and/or $\tilde{u}_s$, both of which are species (and time) dependent. When including charge exchange and/or ionisation collisions, one must evaluate the neutral pdf on the ion velocity grid and vice versa. To achieve this when using one of the aforementioned velocity coordinates, one must interpolate to obtain it. When using the Chebyshev discretisation, a Chebysev spectral method is used to perform the interpolation; when using finite differences, a cubic Hermite spline is used. Note that this interpolation is only necessary when evolving the parallel flow and/or parallel pressure separately from the distribution function.

### *6.5. Wall boundary conditions*

Note that the boundary condition (58) for the neutrals at $z = 0$ for $v_\parallel > 0$ depends on the neutral distribution function at $z = 0$ for $v_\parallel < 0$ through $\Gamma_0$. This distribution function requires specification of the neutral boundary condition at $z = L_z$ for $v_\parallel < 0$, which itself depends on the distribution function at $z = L_z$ for $v_\parallel > 0$. Were one to employ an implicit time advance algorithm, a response matrix or iterative approach would be required to address this inter-dependence. For the explicit time advance employed in the code, this inter-dependence is straightforward to accommodate.

The procedure employed is to first solve for $f_s(z, v_\parallel, t_{m+1})$ at all $(z, v_\parallel)$ locations except for $(z = 0, v_\parallel > 0)$ and $(z = L_z, v_\parallel < 0)$. As the time advance is explicit, this can be achieved given $\{f_s(z, v_\parallel, t_m)\}_{s=i,n}$. The solutions for $f_s(z = 0, v_\parallel < 0, t_{m+1})$ and $f_s(z = L_z, v_\parallel > 0, t_{m+1})$ are then used to compute $\Gamma_0(t_{m+1})$ and $\Gamma_{L_z}(t_{m+1})$. These fluxes can then be used in Eq. (58) to compute the boundary values $f_n(z = 0, v_\parallel > 0, t_{m+1})$ and $f_n(z = L_z, v_\parallel < 0, t_{m+1})$. This procedure is the same for all variants of the drift kinetic and moment kinetics models.

For the models in Sec. 3 where the parallel flow is advanced via force balance, the parallel velocity coordinate is shifted relative to the true parallel velocity $v_\parallel$ by the parallel flow velocity $u_s$. As noted in Sec. 4, this introduces a numerical difficulty: The wall boundary conditions depend on which side of the $v_\parallel = 0$ boundary one is on, but this boundary shifts around in time when using the peculiar velocity as a coordinate. Consequently, a given $w_\parallel$ value may correspond to $v_\parallel > 0$ at time level $m$ and to $v_\parallel < 0$ at time level $m + 1$. If taking the time derivative of the pdf at fixed $w_\parallel$, one will necessarily be mixing regions of phase space on either side of the $v_\parallel = 0$ boundary via time-stepping. This makes enforcement of, e.g., the zero-incoming boundary condition for ions (81) challenging if not infeasible. In the absence of a solution to this problem, the use of the peculiar velocity as a coordinate for the ions or neutrals should be avoided for the open-field line region of the plasma.

It is worth noting that in order to ensure the conservation of the field-line-averaged, species-summed density (as shown in Sec. 4), care must be taken to ensure that the properties $\int_0^\infty dv_\parallel v_\parallel f_{Kw} = -\int_{-\infty}^0 dv_\parallel v_\parallel f_{Kw} = 1$ are exactly satisfied by the numerics. This is achieved in our case by first obtaining the numerical approximation to these integrals and then defining a modified $f_{Kw}$ that is normalised by this result.

## 7. Numerical results

In this section we present data demonstrating that our numerical implementation of the model equations given in Sec. 5 is able to reproduce analytical benchmarks, to preserve the desired conservation properties and to produce physically sensible results.

### *7.1. Linear Landau damping of a sound wave*

As a first test of the code, we consider the linear Landau damping of a sound wave for a closed-field-line system (periodic boundary condition in $z$) with charge exchange collisions between ions and neutrals, but no ionisation. We initialise the distribution function for species $s$ to be of the form

$$f_s = \frac{n_s}{\sqrt{\pi}} \left( \frac{m_s}{2 \left\langle T_{\parallel,s} \right\rangle} \right)^{1/2} \exp\left( -\frac{m_s v_\parallel^2}{2 \left\langle T_{\parallel,s} \right\rangle} \right), \tag{141}$$

with $n_s = \langle n_s \rangle + \delta n_s$ and $T_s = \left\langle T_{\parallel,s} \right\rangle + \delta T_{\parallel,s}$, with the angled brackets denoting a field line average. The piece of the temperature that varies along $z$, $\delta T_{\parallel,s}$, is initially zero, and

$\delta n_s$ is chosen to be small compared to $\langle n_s \rangle$: $\max(\delta n_s(z, t = 0)/\langle n_s \rangle (t = 0)) = 0.001$. The system of equations (1)-(4) can thus be linearised to a good approximation. This facilitates comparisons with the linear analytical theory for this system, presented in Ref. [5].

For all cases shown here, $\langle n_i \rangle = \langle n_n \rangle = N_e/2$ and $\langle T_{\parallel,i} \rangle (t = 0) = \langle T_{\parallel,n} \rangle (t = 0)$. Both the electron-ion temperature ratio and the charge exchange collision frequency are varied, and damping rates and frequencies are extracted by considering the time evolution of the spatially-varying component of the electrostatic potential, $\delta\phi$. In particular, a least-squares fit for $\delta\phi(t)/\delta\phi(t_0)$ is done for each simulation to a function of the form $\exp(\gamma(t - t_0)) \cos(\omega t - \varphi)/\cos(\omega t_0 - \varphi)$ to obtain the damping rate $-\gamma$, frequency $\omega$ and phase $\varphi$. The results for solving the standard drift kinetic system of equations (93)-(96) are given in Fig. 6. There is excellent agreement across a wide range of temperature ratios and charge exchange collision frequencies, both for the damping of finite frequency modes (corresponding to the solid lines) and to a zero frequency mode that appears at larger collisionalities (dashed-dotted lines).

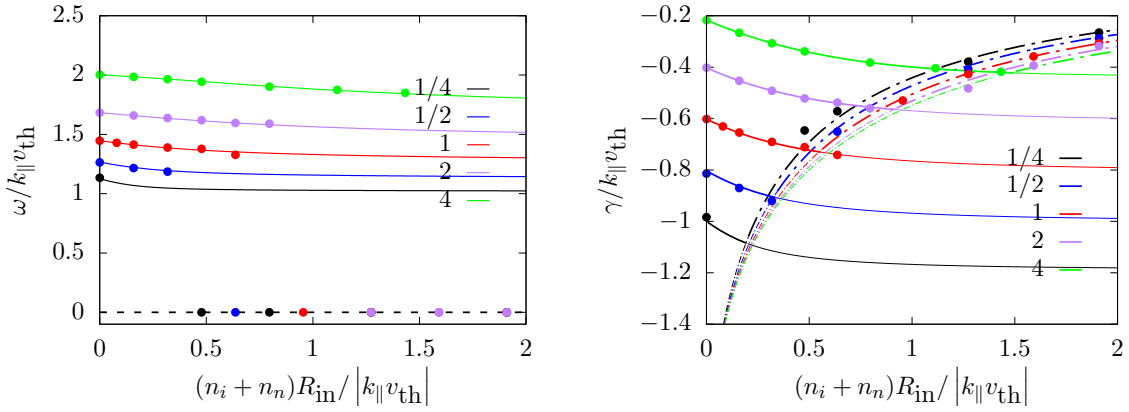


**Figure 6.** Normalized growth rate and real frequency as a function of the ion-electron temperature ratio.

The minor discrepancies between the analytical and numerical damping rates that are apparent for a handful of the cases are due to the simultaneous presence of both modes with similar damping rates. This necessitates in some cases resolving the damping of both modes over many orders of magnitude before the least damped mode dominates the numerical solution – a challenging task given the ever-increasing filamentation of the velocity space due to phase mixing. This should be possible to eliminate by carefully initialising the simulation so that only the least damped mode is present, though we have not yet attempted this. An example of a case in which both modes are present, as well as a case in which they are not, is given in Fig. 7.

We present results in Fig. 8 for the same case with $T_{\parallel,s}(t = 0) = T_e$, but with all of the low-order moments (density, parallel flow and parallel pressure) evolved separately from the pdf (see Secs. 3.4 and 5.4 for details of the model equations). There is again

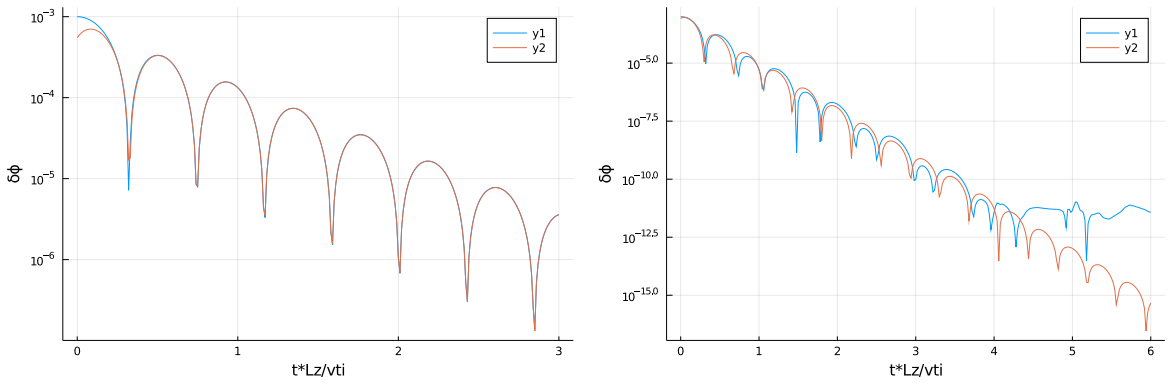


**Figure 7.** Time evolutions of the absolute value of the spatially-varying electrostatic potential $\delta\phi$ (blue) and the result of a least-squares fit (orange) to obtain the damping rate, frequency and phase. The left plot corresponds to $T_e/T_{\parallel,i} = 2$ and $\tilde{R}_{\rm in} = 0$, and the right plot corresponds to $T_e/T_{\parallel,i} = 1$ and $\tilde{R}_{\rm in} = 4$ ($\approx 0.7$ in terms of the normalised frequency used in Fig. 6).

good agreement across a wide range of charge exchange collision frequencies. We note that the results obtained with separate evolution of only the density (Secs. 3.1 and 5.1) and of only the density and parallel flow (Secs. 3.2 and 5.2) are almost identical to the ones presented here in which all three of the lowest-order moments are evolved separately. Testing of the case in which density and parallel pressure are evolved separately is ongoing. The results reported here were obtained using the conserving corrections given by Eqs. 137 and 139.

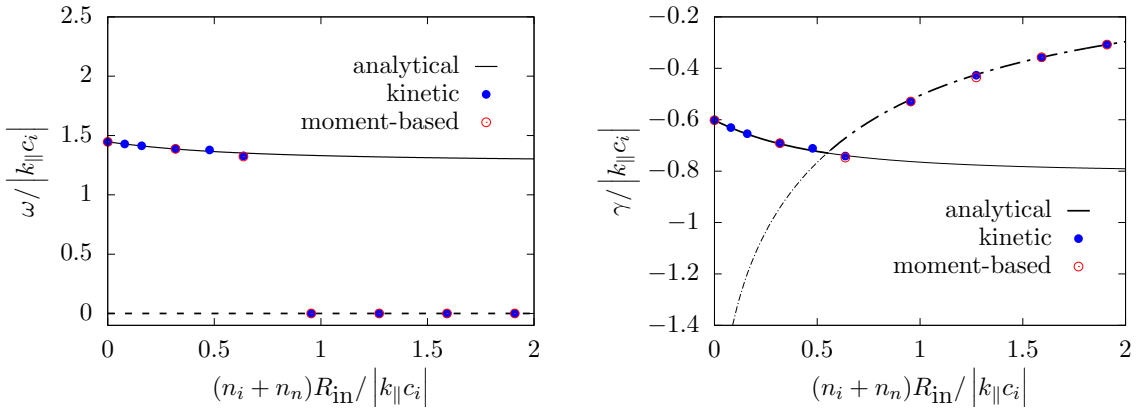


**Figure 8.** Normalized damping rate and real frequency as a function of the charge exchange collision frequency for cases with $\langle T_{\parallel,s}\rangle = T_e$. The 'kinetic' model refers to the standard drift kinetic system of equations, while the 'moment-based' model is one in which density, parallel flow and parallel pressure are evolved separately from the modified pdf.

In Figure 9 we show the difference in conservation properties between cases for which the conservative corrections of Eqs. (137) and 139 are employed and those for

which no conserving correction is applied. With the conservative implementation, all of the requisite moments of the modified distribution function are conserved to machine precision, regardless of numerical resolution.

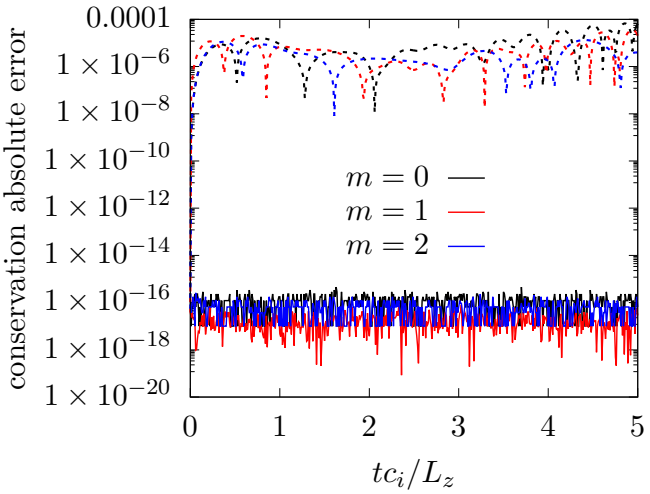


**Figure 9.** Time traces of the deviation from exact conservation of the moments $\int d\hat{w}_\parallel \hat{w}_\parallel^m \hat{g}$ for low-resolution ($N_z = 9$ on one element, $N_v = 9$ on five elements) simulations with normalised $R_{\rm in} \approx 0.3$. Solid and dotted lines correspond to simulations with and without conserving corrections, respectively.

### *7.2. Plasma on open field lines: analytical comparison*

We next compare our simulation results to the analytical solution presented in Sec. 4.1. As argued in Sec. 6.5, the moment-kinetic models in which the parallel flow are evolved are not conducive to simulations of plasma on open field lines. Consequently, we restrict our attention to the drift kinetic model here. A demonstration of the other moment kinetic approaches (in which only the density or both the density and parallel pressure are separately evolved) for open field line regions is underway.

The ion equation being solved in the code for the standard drift kinetic model is

$$\frac{\partial \tilde{f}_i}{\partial \tilde{t}} + \tilde{v}_\parallel \frac{\partial \tilde{f}_i}{\partial \tilde{z}} - \frac{1}{2}\frac{\partial \tilde{\phi}}{\partial \tilde{z}}\frac{\partial \tilde{f}_i}{\partial \tilde{v}_\parallel} = \tilde{R}_{\rm ion}\frac{c_s}{v_\delta}\exp\left(-\tilde{v}_\parallel^2\frac{c_s^2}{v_\delta^2}\right), \tag{142}$$

where we have approximated $\delta(v_\parallel) \approx (1/\sqrt{\pi}v_\delta)\exp(-v_\parallel^2/v_\delta^2)$ with the proviso that $v_\delta \ll c_s$. In terms of normalised quantities, the solution (76) is

$$\tilde{z} = \frac{1}{2} \pm \frac{2}{\pi \tilde{R}_{\rm ion}} D\left(\sqrt{-\tilde{\phi}}\right). \tag{143}$$

For our benchmark simulation, we use a Chebyshev pseudo-spectral method in both $z$ and $v_\parallel$. The $z$ grid consists of two $z$ elements, each containing nine grid points, and the $v_\parallel$ grid consists of ten elements, each containing seventeen grid points. The wall

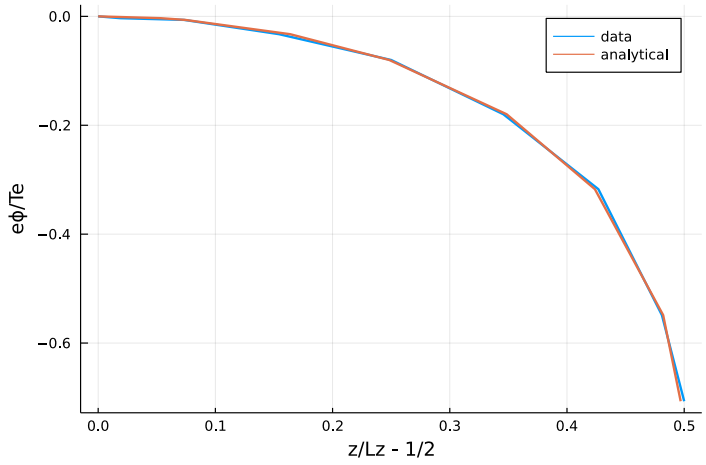


**Figure 10.** The steady-state electrostatic potential profile obtained by solving Eq. (142) (blue line) and by using the analytical solution of Eq. (143) (red line).

temperature $T_w$ is taken to be equal to $T_e$, the source width parameter is $v_\delta = 0.5c_s$, $\tilde{R}_{\rm ion} = 0.688$ and the ions are initialised to a Maxwellian velocity distribution with initial temperature $T_e$ and an initial density with Gaussian distribution in $z$. The resulting steady-state solution for $\tilde{\phi}(\tilde{z})$, along with a comparison to the analytical solution (143) is given in Fig. 10.

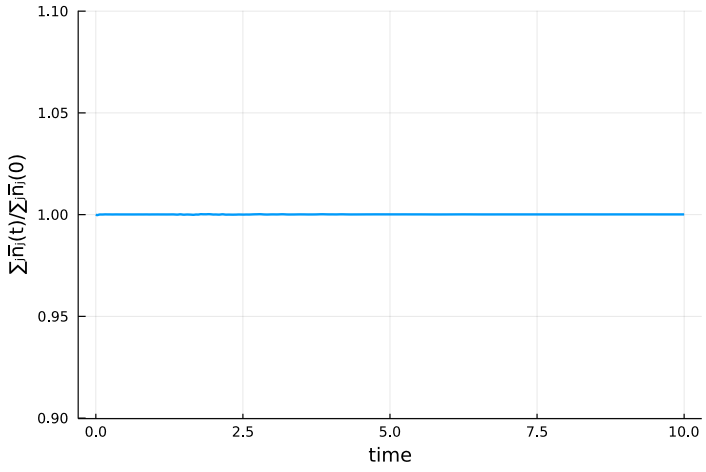


**Figure 11.** Time trace of the species-summed, line-averaged density, normalised by its initial value.

### *7.3. Plasma on open field lines: physics study*

We finally consider the drift kinetic system of equations given in Sec. 5. We take the normalised collision frequency factors to be $\tilde{R}_{\rm ion} = \tilde{R}_{\rm in} = 2$ and otherwise use the same

numerical parameters and initial conditions as we did for the analytical benchmark, except that we use eight $z$ elements rather than two. A cross-section of the numerical results are presented in Figures 11-13. In Fig. 11 we consider the evolution of the species-summed, line-averaged density. As shown in Sec. 4.1, this density should be conserved, and this is indeed the case in the simulation to machine precision. The steady-state electrostatic potential and particle distribution functions for ions and neutrals are given in Figs. 12 and 13. As might be expected, the loss of electrons to the walls gives rise to an electric field that pulls ions out of the simulation domain. These ions are replaced by neutrals traveling back into the simulation domain, leading to the regions of high neutral density near the walls (with neutral velocities away from the walls) visible in Fig. 13. The phase space structure in the ion distribution function is likely a result of the ionisation of neutrals in the high-density regions near the walls, followed by an acceleration of these ions towards the nearest wall. This reduces their initial speed away from the walls and eventually changes their direction of motion and accelerates them into the wall near which they were generated. Conversely, ions generated sufficiently far from the nearest wall can cross the symmetry point in $z$ and are accelerated towards the wall furthest from where they were generated.

As an aside, we note that the kinetic Bohm criterion, which for the case of Boltzmann electrons can be written [6]

$$\int dv_\parallel \frac{c_s^2}{v_\parallel^2} f_i(v_\parallel) \leq 2n_i, \tag{144}$$

is satisfied for this simulation.

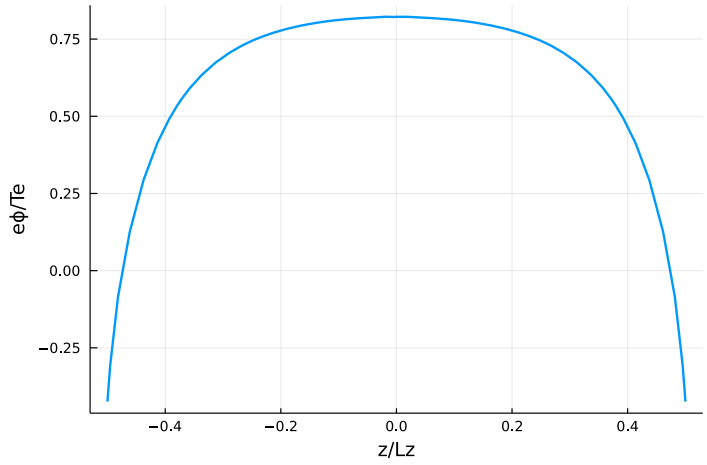


**Figure 12.** Electrostatic potential profile in steady state.

## 8. Conclusions and future plans

There are a few conclusions that can be drawn based on our results. First, the standard drift kinetic system of equations described in Secs. 2, 4 and 5 is generally well-behaved

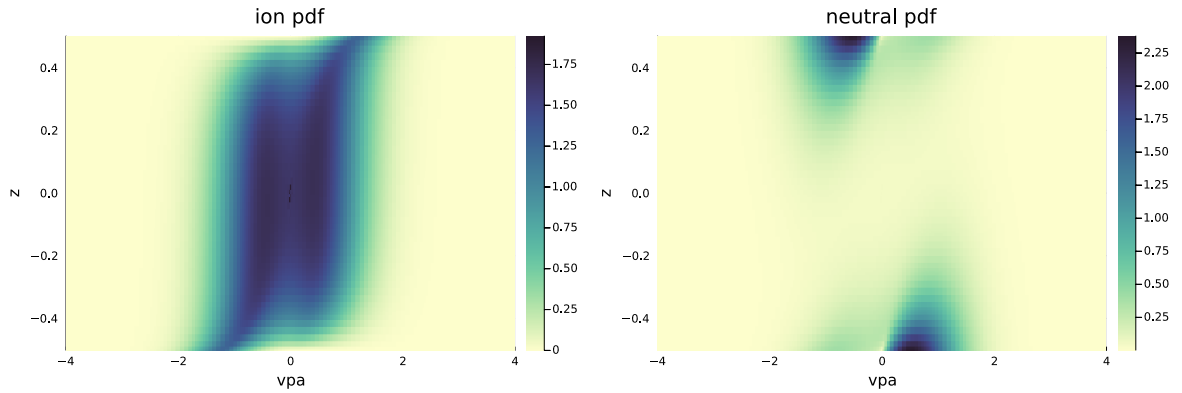


**Figure 13.** Phase space portraits of the steady-state, normalised ion (left) and neutral (right) particle distribution functions, $\tilde{f}_i$ and $\tilde{f}_n$.

both for periodic and wall boundary conditions in $z$. Care should be taken where possible to ensure that the desired conservation properties are preserved by the numerical scheme, and we have outlined ways in which this can be achieved. Second, the moment kinetic model variants in which the peculiar velocity is used as a coordinate give rise to numerical difficulties when enforcing wall boundary conditions. In the absence of solutions to these difficulties, use of these particular moment kinetic models in not recommended for the plasma in open field line regions.

The other moment kinetic model variants – in which only the density or both the density and parallel pressure are evolved for the ions and neutrals – should work for both open and closed field line regions. We have verified this to be the case for the model with only density evolution, but our work on the case with density and parallel pressure evolution is ongoing. In all cases with the moment kinetic models, we found it important to apply the conserving corrections detailed in 6.3. In addition to ensuring conservation to machine precision, we found that application of these corrections enhanced numerical stability.

The advantages of evolving only the density separately are unclear: such a model cannot work as a standalone fluid model, even in the collisional limit, and it does not possess the property that the velocity is normalised to a local thermal speed. The model in which the parallel pressure is also evolved does possess this latter property, which may make it worth further exploration in both the 1D and 2D settings. Consequently, our current thinking is that the best model for ions and neutrals is either the standard drift kinetic model or the moment kinetic variant in which both density and parallel pressure are evolved.

The immediate plans going forward should be to extend this work to a two-spatial-dimension system consisting of a helical magnetic field and to implement a fluid model for electron dynamics. The latter will allow for a more realistic solution for the electrostatic potential than that provided by the Boltzmann response of Eq. (4).

[1] M. Barnes, F. I. Parra, and M. R. Hardman. Numerical study of 1d drift kinetic models with periodic boundary conditions. *Excalibur/Neptune Report*, 2:2047357–TN–01–02 M2.1, 2021.

[2] M. Barnes, F. I. Parra, M. R. Hardman, and J. Omotani. Numerical study of 1+1d, moment-based drift kinetic models with periodic boundary conditions. *Excalibur/Neptune Report*, 4:2047357–TN–01–02 M2.2, 2021.

[3] M. Barnes, F. I. Parra, M. R. Hardman, and J. Omotani. Numerical study of 1+1d, moment-based drift kinetic models with periodic boundary conditions. *Excalibur/Neptune Report*, 6:2047357–TN–01–02 M2.3, 2021.

[4] M. Barnes, F. I. Parra, M. R. Hardman, and J. Omotani. Numerical study of 1+1d drift kinetic model with wall boundary conditions. *Excalibur/Neptune Report*, 8:2047357–TN–02 M2.4, 2021.

[5] F. I. Parra, M. Barnes, and M. R. Hardman. 1d drift kinetic models with periodic boundary conditions. *Excalibur/Neptune Report*, 1:2047357–TN–01–02 M1.1, 2021.

[6] E. R. Harrison and W. B. Thompson. The low pressure plane symmetric discharge. *Proc. Phys. Soc.*, 74:145, 1959.

[7] N. H. Abel. *Journal für die reine und angewandte Mathematik*, 1:153, 1826.

[8] C.-W. Shu and S. Osher. Efficient implementation of essentially non-oscillator shock-capturing schemes. *J. Comp. Phys.*, 77:439–471, 1988.

[9] S. Gottlieb and C.-W. Shu. Total variation diminishing runge-kutta methods. *Mathematics of Computation*, 67:73–85, 1998.

[10] S. Gottlieb, C.-W. Shu, and E. Tadmor. Strong stability-preserving high-order time discretization methods. *SIAM Rev.*, 43:89, 2001.

[11] D. R. Durran. *Numerical methods for fluid dynamics*. Springer, 2010.

[12] M. Abramowitz and I. A. Stegun. *Handbook of Mathematical Functions with Formulas, Graphs, and Mathematical Tables*. Dover, New York, 1972.

[13] Matteo Frigo and Steven G. Johnson. The design and implementation of FFTW3. *Proceedings of the IEEE*, 93(2):216–231, 2005. Special issue on "Program Generation, Optimization, and Platform Adaptation".

[14] C. W. Clenshaw and A. R Curtis. A method for numerical integration on an automatic computer. *Numerische Mathematik*, 2:197, 1960.